Note NA62-21-04

CERN-ACC-NOTE-2021-0013

CERN-PBC-Note-2021-001

2021-04-30

Lau.Gatignon@cern.ch

Considerations for a RF separated K^+ beam for NA62

R.Appleby[1,2], J.Bernhard[3], G.Burt[1,4], J.Dainton[1,4], L.Gatignon[3,4,+], E.Goudzovski[5], R.Jones[1,4], C.Lazzeroni[3,5], A.Romano[5], G.Ruggiero[3,4], S.Tygier[2,*]

1 *Cockcroft Institute, Daresbury, UK*
2 *Manchester University, Department of Physics and Astronomy, UK*
3 *CERN, Switzerland*
4 *Lancaster University, Physics Department, UK*
5 *University of Birmingham, School of Physics and Astronomy, UK*
❊ *Now at Rutherford Lab*
\+ *Email: Lau.Gatignon@cern.ch*

Keywords: Conventional Beams, Beam Optics, Beam Transfer, North Area, Radio-Frequency

Abstract

In this document we assess the potential of RF separation to increase the kaon content of the high-intensity secondary beam to the NA62 experiment in the CERN North Area. The present mixed beam provides a nominal kaon flux of 45 MHz out of a total beam intensity of about 750 MHz. The experiment wishes to increase the kaon flux, without too much increasing the overall beam intensity which might otherwise exceed the rate capability of several detectors and cause increased backgrounds to the detector.

To avoid a strong reduction of the kaon flux by decays in a very long beam line, a compact RF separator approach is evaluated as a baseline. Alternative possibilities are briefly described at the end of the document. It turns out that the performance will not meet expectations and that therefore conventional methods to increase the beam intensity will have to be pursued. With the relatively short length proposed, the πK phase difference is too small to separate the kaons from the large emittance mixed beam. A larger phase difference would imply more length and hence a drastic reduction of the kaon component due to decays.

1. Introduction

The NA62 experiment [1] aims to measure the branching ratio of the very rare decay $K^+ \rightarrow \pi^+ \nu\bar{\nu}$ to high precision. The Standard Model prediction for the branching ratio of this decay mode [2] is small but known with good precision: $(8.4 \pm 1.0)\ 10^{-11}$. The present beam line, called K12, produces a mixed beam of instantaneous intensity 750 MHz with a K^+ component of 6%, i.e. about 45 MHz. The presently approved experiment is designed to collect 100 signal events, allowing a 10% measurement [3]. An eventual second phase would aim at a 5% precision, requiring a 4-fold increase of beam intensity. As the detectors measuring the incoming K^+ parameters are exposed to the full beam, it is considered a real advantage if the kaon fraction in the beam can be increased significantly. The non-kaon component also contributes to background rates in the detectors, e.g. through pile-up and via interactions with material close to the beam or with rest gas in the beam line and decay volume. At high energy RF separation between kaons and mainly protons, pions and positrons seems the most promising approach to enrich the kaon component. RF separated kaon beams at medium and high energies have been used in the past, but never at the intensities required for the present application. In this work we investigate if a RF separated beam can fulfil the requirements in terms of intensity, purity and beam momentum required.

RF separation takes advantage of the difference in speed for particles of different mass at the same momentum. This causes a difference time of flight between two transverse RF cavities and therefore different deflections. This is most effective at lower momentum, where the difference in speed is greater. This document discusses two methods for separation, specifically for the case of cleaning unwanted protons, positrons and pions from a kaon beam. The high efficiency method which provides strong cleaning of two unwanted species but has strict constraints on length. And a compact method, which is less effective but requires less space.

Both methods have a similar overall layout as shown in Figure 1, the only difference being the collimator being replaced by a dump in case the wanted particles (K^+) receive a kick and the unwanted ones (π^+ and p) go straight. The mixed beam is produced at a target to the left and must be collimated both transversely and in momentum, then matched into the first cavity in the pre-match section. Between the two cavities is a delay line, which needs to be long enough for the speed difference to result in a RF phase differences at the second cavity. After the second cavity a post line is needed in order for the change in particle angle to develop into a change in position, before a collimator can be used to remove unwanted particles. The remaining particles can then be used in the experiment.

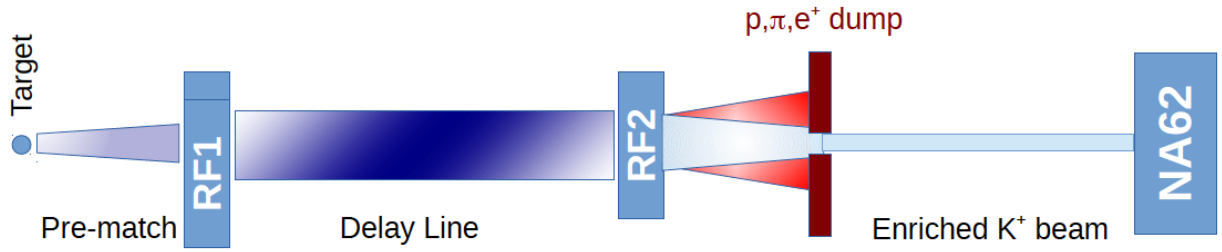

Figure 1: *Basic scheme of the RF separated beam line for the case where the wanted particles go straight through a collimator slit.*

The difference of arrival time between particles is considered to be random and much longer than the RF cycle. It is therefore not sufficient for the scheme to only work for particles that arrive at the first cavity with a special phase. This limits maximum efficiency of the scheme. A more advanced Lissajous scheme which uses both horizontal and vertical transverse kicks from additional cavities can overcome this, but is not considered here.

1.1 High efficiency method

The high efficiency method uses an arrangement of RF cavities that allows equal RF deflections to the two main species of unwanted particles (pions and protons), while at the same time giving a different deflection to the wanted particles. This requires the time of flight difference between the two unwanted species to be an integer number of RF periods. For a given beam momentum and RF frequency the first suitable inter-cavity distance is exactly specified. For example, at 75 GeV, with a 3.9 GHz cavity the distance required is close to 1 km.

Given the random arrival times of the particles, the resulting deflection of particles will be a function of their arrival phase at the first cavity. Some of the deflected species will receive no net deflection. If the goal is a high purity beam, it is therefore beneficial to set the cavity phases such that the wanted particles receive a net kick and the unwanted particles have their kicks cancel. This allows almost all unwanted particles to be stopped by a collimator placed on the beam axis, as only the wanted species have the possibility to receive a large enough kick to bypass it. If instead the net kick were given to the unwanted particles and large amplitude particles were collimated, then some unwanted particles would always be able to pass through.

To be effective the separator must cause a shift in the phase-space position of the beams relative to each other, such that unwanted particles can be collimated without losing wanted particles. This shift must be large compared inherent spread of the beam. The deflection is in the angle of the particles, and so must be compared to the angular spread of the beam.

As areas in phase space are conserved by Liouville's theorem, reducing the angular spread results in a larger beam position width. The ability to reduce the angular spread is therefore limited by the physical aperture of the RF cavity.

1.2 Compact method

The short method drops the strict condition that both unwanted species are given an equal deflection. Instead it tries to give the best possible cleaning in a given available space. In this case the deflection difference is not maximal, however it still allows selective collimation of some particle species.

In this case it is preferable to close the RF bump for the kaons while allowing the protons and pions to receive a net kick. Now the collimator is used in a traditional way, removing high amplitude particles. This allows a high transmission of kaons, and can give a good removal of protons. But the pions to not receive as strong a deflection and so not as efficiently cleaned.

As a baseline for the RF system we consider using 3.9 GHz transverse deflecting cavities, with a gradient of 5 MeV/c per metre and total deflection of 15 MeV/c. The free aperture diameter is 2.7 cm . We also consider the possible improvement achievable with a 5 GHz cavity.

A higher RF frequency would reduce the required length of the separation system as there would be a larger phase shift for a given time of flight difference. For example, a 9 GHz X-band has been considered, however due to the long spill length the cavity heat load would be too great. Resistance of superconducting RF scales with the square of frequency, and will already be challenging at 3.9 GHz. However, different technologies may be considered for frequencies up to 12 GHz.

1.3 Constraints for a NA62 future beam design

In this document we describe an attempt to design a possible optics for the secondary beam, considering the various requirements:

1. At high energy, the required frequency f depends on the beam momentum p and the distance L between the cavities via $\Delta\phi = 2\pi\,[Lf(m_1^2 - m_2^2)/2cp^2]$ where $\Delta\phi$ is the phase difference accumulated over a distance L between two particles of rest mass m_1 and m_2. $\Delta\phi$ depends on the separation strategy (see below). If one wants to create a phase difference of multiple RF periods between pions and protons (to dump both of them), the length for a 75 GeV/c beam would be quite long.
2. The present NA62 beam operates at 75 GeV/c, but any momenta between 60 and 75 GeV/c are considered acceptable. At 75 GeV/c the distance between the cavities must be almost 1 km to equalise the phases for π and p at 3.9 GHz. Clearly X-band cavities are called for.
3. Kaons have an average decay length of 7.52 metres per GeV/c. Therefore, it is important to keep the beam line as short as possible.
4. The NA62 experiment wants a significant enrichment, but does not aim for ultimate purity. A purity of 20 or 30% would already constitute a very significant improvement.
5. As NA62 wants to significantly increase the K^+ flux (ideally x4), losses of kaons along the beam line must be minimised. As the acceptance of the present K12 beam is already maximised, the main parameter for any K^+ flux increase can only be the primary proton flux. The overall extracted intensity to the North Area limits the proton flux on the kaon production target T10 to 2 10^{13} protons per spill, if some beam must be delivered also to the EHN1 and EHN2 halls. This is factor ≈ 6 higher than the present nominal flux for NA62. The hope is that this will compensate for the losses due to RF and K^+ decay losses along the beam.
6. The kaon component is tagged by the so-called KTAG Cerenkov detector, based on the CEDAR principle. This requires the beam angular spread to be below 100 microradians RMS at 75 GeV/c (this constraint is slightly more relaxed at lower momenta).
7. The beam size at the Gigatracker, GTK, must fill the detector size as uniformly as possible to keep the instantaneous intensity per pixel at an acceptable level.
8. The beam size and angular spread in the main NA62 detectors must match the dimensions of the central holes in the detectors. Losses on the way cause backgrounds and must therefore be minimised.
9. Radiation protection constraints are stringent and must be respected rigorously. This is in particular an important constraint around the primary target and primary proton dump, as well as for muons above and behind the beam line and detectors.
10. Last but not least, the beam line must be compatible with the geometry of the existing tunnel. This turned out to be a complication for the beam optics, but a possible solution is described in chapter 3.

2. The RF separation approach for NA62

The RF system design is for the moment based on the ILC crab cavities [4]. They operate at 3.9 GHz, but this could be increased to 5 GHz without major costs and without compromising operation at a high duty cycle as for the SPS flat top, e.g. 4.8 seconds every 16.8 seconds.

These cavities have a large iris size (30 mm diameter, allowing for 27 mm diameter free passage, considering the sagitta of the deflected particles), but the RF voltage is 'only' 5 MV/m. Therefore a 3 m cavity gives a transverse kick of 0.2 mrad at 75 GeV/c, or 0.25 mrad at 60 GeV/c. The angular divergence of the beam at the cavity location must be small or the cavity must be extremely long to ensure that the kicked beam at the end of the RF system separates sufficiently from the un-kicked beam envelope. This calls for a parallel beam, which is therefore large, but the size can hopefully still be matched to the iris size and a good compromise must be found. It turns out that 3 m of cavity is too small for our case and we assume for the moment 6 m of cavity in both locations. We assume the kick to be horizontal.

After the second cavity, RF2, the beam will be focused onto a collimator with a small slit. The RF phase and frequency will be based on the compact RF separator design, not optimal for separation but shorter. As we are aiming for maximum flux and not for the best purity, we suggest to minimise the kick to the K^+ and have a larger maximum kick for the unwanted particles. The delay line between RF1 and RF2 will be too short to have strong separation, anyway.

The present study proposes a possible beam optics, matching the tunnel geometry, see Chapter 3. Based on a simulation of the beam characteristics, presented in Chapters 4 and 5, we estimate in Chapter 6 the possible performance of the separator in terms of transmission and enrichment. Alternative options for RF enrichment are briefly addressed in Chapter 7 before concluding in Chapter 8.

3.The optics design

The beam line for NA62 consists of a primary proton line, called P42, of length 838 metres and the secondary mixed beam K12 of length 267 m. They are part of the so-called P0 complex, schematically shown in Figure 2.

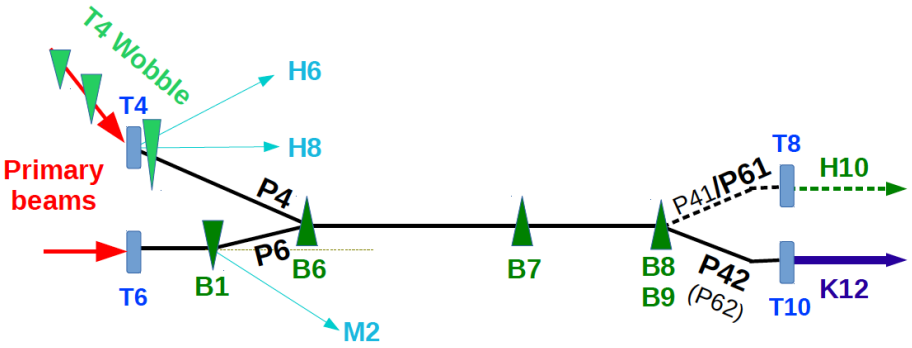

Figure 2: *Schematic view of the P0 complex (not to scale)*

The new beam line will need a new primary target somewhere along the P42 line. This target will become the start of the new RF-separated K^+ beam schematically depicted in Figure 1. The geometry of the more relevant part of P42 for the present studies is shown in Figure 3.

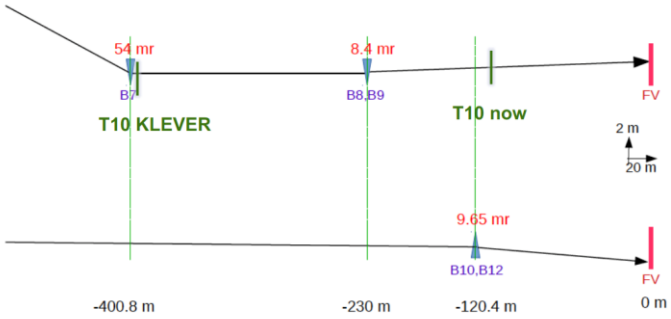

Figure 3*: The geometry of the relevant part of the P42 beam line. FV indicates the start of the NA62 fiducial volume. The horizontal plane is shown at the top, vertical plane at the bottom. In the horizontal plane deflections to the Jura side are towards the top of the diagram*

The beam follows a tunnel which has a big - 54 mrad - deflection at BEND7 (consisting of a series of nine 5 metres long dipoles), a second, smaller, horizontal bend at BENDs 8 and 9 and a vertical deflection (roughly 9.6 mrad downward) at BENDS 10, 11, 12 that renders the beam horizontal into the direction of the NA62 detectors.

Various locations for the new primary target have been discussed with the radiation protection experts at CERN. Any option in which the target would be followed by the same front-end as the present K12 beam, i.e. a quadrupole triplet and an achromat with a proton dump in the middle, is considered extremely problematic by radiation protection. Muons would essentially go straight and cause very high muon doses in the environment, e.g. at the level of the Lion river. They would also cause high backgrounds at the COMPASS location. The option which for the moment seems possibly less problematic is the one where the target would be installed at the beginning of the present BEND7. This bend would be modified (for the - much lower - kaon beam momentum) and the primary protons and many of the muons would then naturally be directed towards the ground shield between the M2 and P42+K12 lines. This option remains to be studied by radiation protection.

Such a layout requires a complete redesign of the front-end of the beam. The front-end has to ensure maximum angular acceptance and a momentum definition with sufficient resolution. The general principle of momentum definition is illustrated in Figure 4 and explained in [5]. For the moment a momentum band of ≈ 1% RMS is assumed to be adequate. A reduction of the momentum band leads to a proportional reduction of kaon flux. A larger momentum band smears the phase difference between RF1 and RF2 and would also cause significant chromatic aberration.

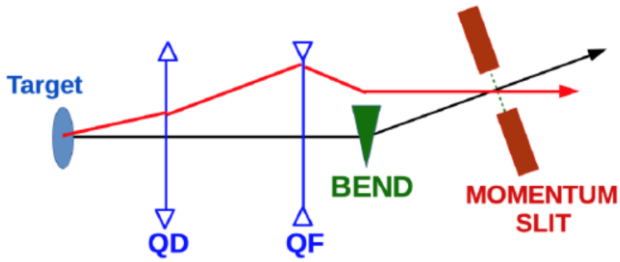

Figure 4: *The principle of the optics of the front end*

In Figure 5 we show in more detail the principle and layout of the front end that we retained initially. The target is followed by a collimator (to stop pions and kaons at large angles before they decay into muons) and then immediately by a quadrupole triplet with the same layout and quadrupole types as the one in the present K12 beam. A vertical corrector allows to adjust the vertical steering, potentially affected by quadrupole alignment. The 54 mrad deflection is made by two large aperture dipoles of MTN type, giving a 27 mrad deflection each. The primary protons that traversed the 400 mm Beryllium target without interacting will be deflected much less and will be dumped in a massive water-cooled collimator with a fixed hole for the beam passage (similar to the TAX in the present beam, but without motorisation: less maintenance). In the middle of this BEND7 section, a quadrupole, focussing from the centre of the first dipole to the centre of the second one and usually called 'field lens', will cancel the dispersion [5]. This technique is also shown in Figure 6. Optionally a radiator (copper or tungsten plate of a few mm thickness) can be installed here, or at a later focal point along the beam line, to reduce the positron content of the beam (8%).

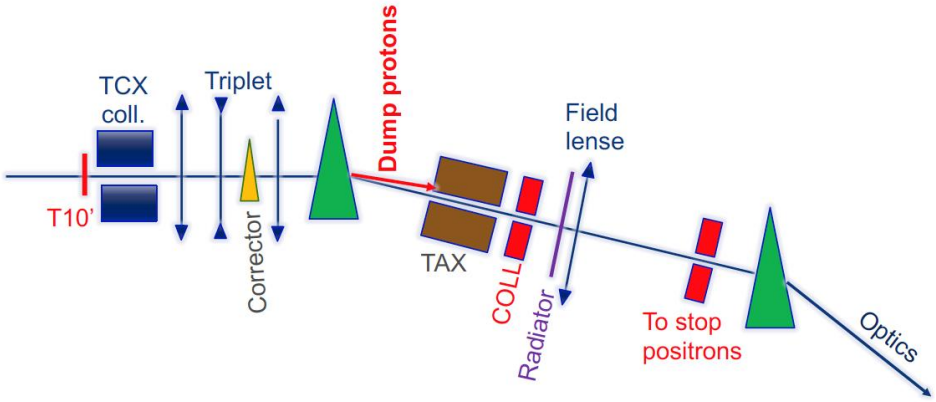

Figure 5: *A schematic view of the new K12 front end. Here deflections to the Jura side are shown towards the bottom of the diagram*

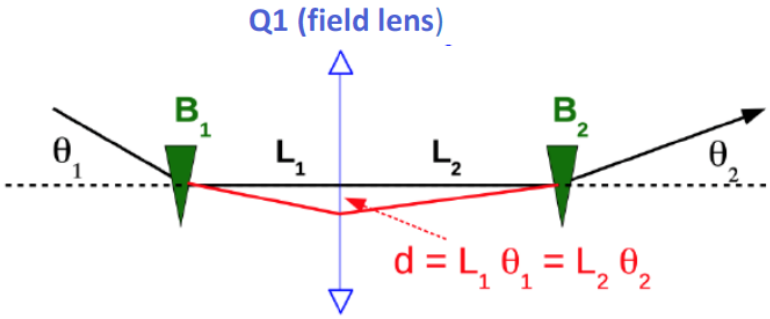

Figure 6: *Explanation of how dispersion can be recombined by focusing in between two dipoles. Note that the two angles θ_1 and θ_2 may be different.*

The momentum slit is finally located immediately downstream of the quadrupole. For optimal momentum resolution the beam should be focused at the momentum slit, but to avoid a steady increase of the cosine like terms (R_{11} and R_{33}), the beam is focused in both planes at the centre of the field lens. The horizontal magnification at that point has been set to 3, which still provides adequate momentum resolution. Stronger focusing (e.g. magnification 1) would lead again to a faster increase of the cosine like waves, which turns out to be hard to manage. The compromise chosen leads to a substantial improvement on the beam characteristics at the first cavity.

A system of 4 quadrupoles makes the beam parallel in RF1 (in both planes) with some margin for fine-tuning. A compromise has been found between divergence (versus kick strength) and beam size (versus iris size).

Assuming that the delay line will provide a one-to-one horizontal image of the RF1 beam at RF2, we matched (as a test) the beam leaving RF1 through the pion/proton/positron dump collimator into the KTAG position with adequate beam size and parallelism. This allowed an estimate of the length required and thus finding the final position of RF2 and therewith the distance between RF1 and RF2. Unfortunately, the position of RF2 ended up at the location of the last vertical bends BEND10 to BEND12. As the beam at the cavity must be parallel, at least in the horizontal plane (the plane of the RF kick). However, the cavity would be preceded by a dipole and then at some distance a very strong quadrupole. In Figure 7 we show what this would imply for the beam incident on that quadrupole. This is clearly not possible and space must be created for some optics in between the bends and the cavity. We decided therefore to reduce the top beam momentum to 60 GeV/c, which allows gaining the minimum space necessary. Finally, the distance between the centres of RF1 and RF2 ends up to be about 270 metres. This distance also favours a lower beam momentum of 60 GeV/c.

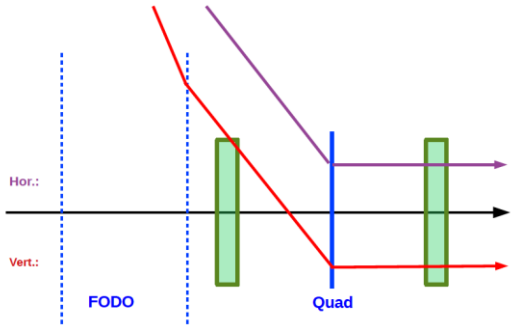

Figure 7: *Illustration of the problem resulting from the presence of the 'field lens' in the vertical bend implies for the optics upstream*

The optics of delay line itself turns out to be non-trivial. In a straight tunnel one would install a simple FODO channel with the required phase advance. However, there are two kinks in the tunnel, which the beam line must follow, see Figure 3. Each of the two kinks is provided by two 1 m long large aperture dipoles. To eliminate the dispersion from such a bend (a necessary condition for NA62), a strong quadrupole (field lens) must be foreseen in between the bends. It must focus from the centre of the first to the centre of the second dipole. This is again the technique shown in Figure 6 and explained in [5].

The angles of deflection in the two bends, θ_1 and θ_2, may be different, but in that case the distances L_1 and L_2 from the centres of the dipoles to the centre of the quadrupole must follow the rule

$$\frac{L_1}{L_2} = \frac{\theta_2}{\theta_1}$$

The strength (integrated gradient: GL) of the quadrupole is given by the focal distance f = 3.3357 p/GL, which varies with section length L = L_1 + L_2 roughly as f ≈ L/4 (thin lens approximation and symmetric system). This turns out to be about three times stronger than a typical GL of a FODO magnet. It is therefore very difficult to use these quadrupoles as part of a FODO lattice. To minimise the effect of these quadrupoles, it was decided to put a focus in both planes at each of these two quadrupoles. The first approach would then be to apply a regular FODO from RF1 to the first of these quads and a second FODO from the first to the second quad. Note that the first FODO starts at a parallel section. Therefore, the phase advance must be 270°. The second delay line has a total phase advance of 360°. However, again the cosine like wave would grow too much. Therefore, in both sections we have played the same trick. We kept the quadrupole and the second dipoles at fixed locations, but moved the upstream dipoles further upstream. Therefore, L_1 and also L and f increase, whereas the GL of the focusing decreases. Details of these considerations are given in Appendix A. We then also increased the spacing in the second part of each FODO channel and decreased correspondingly the spacing in the first part. This is limited by the maximum GL of the upstream FODO quadrupoles, which are large aperture and therefore not so strong quadrupoles of QPL type. We also increased the magnification at the two field lens quads. The net effect is a significant decrease of the cosine like waves later on.

The last vertical bend is immediately followed by a quadrupole doublet that makes the beam parallel at the RF2 cavity in the horizontal plane with the same R_{12} term as at RF1. In the vertical plane the beam is diverging, the only constraint that we could respect is to keep all optical terms within reasonable limits.

A quadrupole triplet then focuses the beam horizontally (not vertically) at the p/π/e^+ collimator, with horizontal magnification 1.0. From there 8 strong quadrupoles allow fine tuning of the beam characteristics at the NA62 KTAG and beyond. An intermediate focus after the fourth quadrupole helps to keep the cosine-like wave under control. Now the beam is strictly parallel at the KTAG, but the beam size has not yet been optimised to match the KTAG requirements and beam size through the NA62 experiment. However, up to 8 quadrupoles are foreseen for this matching and 3 more can be re-tuned if necessary.

The optics of the complete kaon beam line is shown in Figure 8. The optics coefficients are listed in Appendix B and are also available online [6].

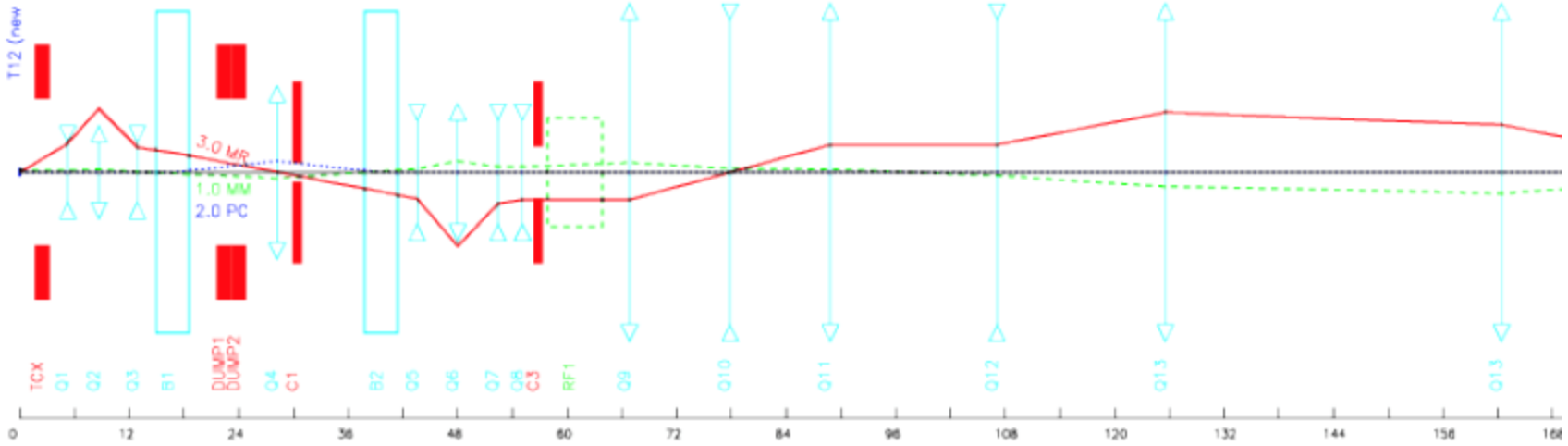

K12RFBEAM – RF SEPARATED K+ BEAM TO NA62

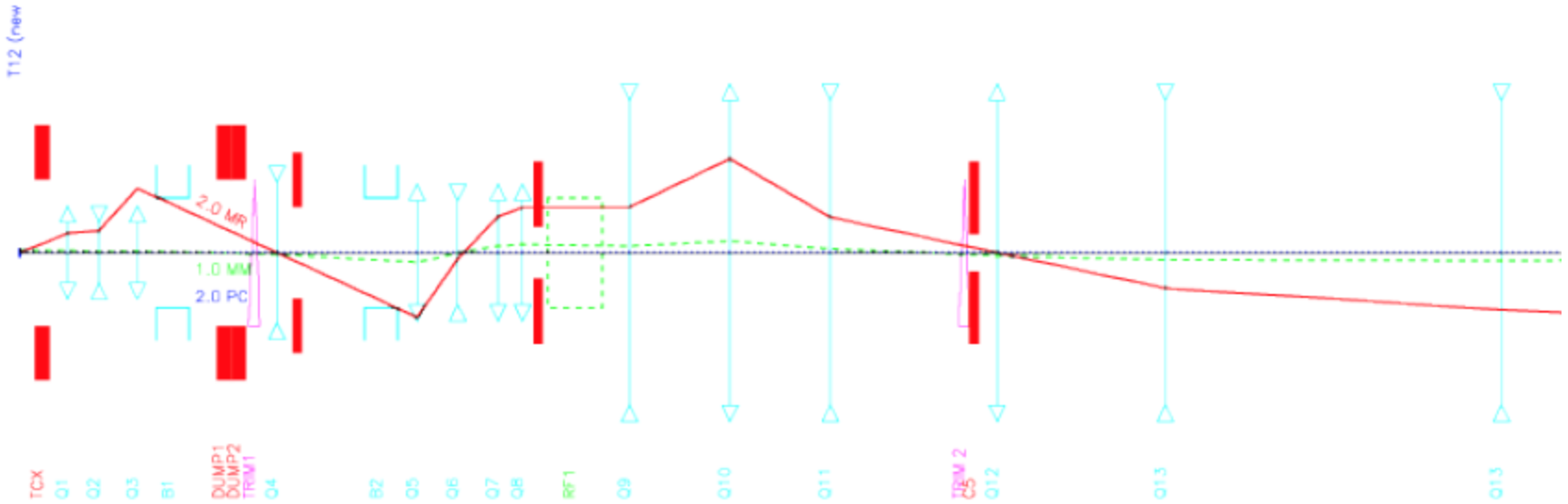

Q29
Q28
RF2
CT.
Q27
Q26
BEND6
MIB
Q25
BEND5
Q24
Q23
Q22
Q21
Q20
Q19
Q18
Q17
Q16
BEND4
Q15
BEND3
Q14
330
318
306
294
282
270
258
246
234
222
210
198
186
174

Q29
Q28
RF2
CB
Q27
Q26
BEND6
MIB
Q25
SCR1
BEND5
Q24
Q23
Q22
Q21
Q20
CB
Q19
Q18
Q17
Q16
BEND4
Q15
BEND3
Q14

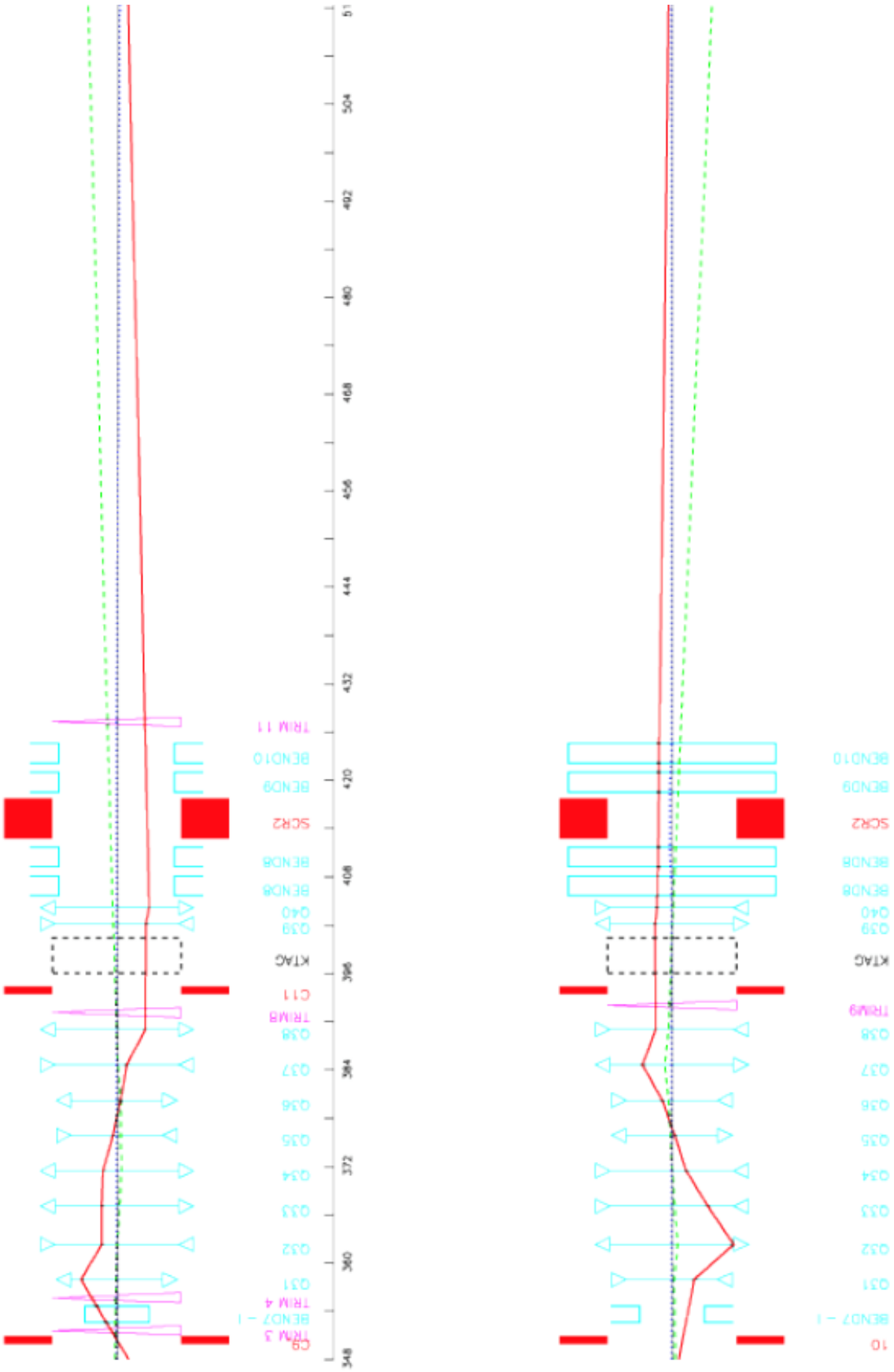

Figure 8: *The present version of the full optics of the RF separated K12 beam line. The red lines indicate the R_{12}, respectively R_{34} terms (mm/mrad), the green lines R_{11} and R_{33} (mm/mm) and the dotted blue lines the dispersion (mm/%)*

4. Simulations for the un-kicked beam

The optics described in the previous chapter has been implemented in the tracking program Decay Turtle [7]. Turtle applies a circular cut at each quadrupole corresponding to the inscribed radius of the aperture. In addition, a simple collimation scheme has been introduced with the following cuts:

- A horizontal gap of ±5 mm at the momentum slit,
- A ±14 mm gap in both planes at the entrance of both RF1 and RF2,
- A ±2 mm gap at the p/π/e+ dump

The overall transmission for stable particles is the same (within a few percent!) as for the present beam to NA62, i.e. ignoring decays and the effect of the lower beam momentum (60 instead of 75 GeV/c). The horizontal angular acceptance is ±3 mrad and the vertical one ±1.6 mrad. In Figure 9 we show the momentum distribution of the beam delivered to the experiment, which has a RMS width of 1.2%.

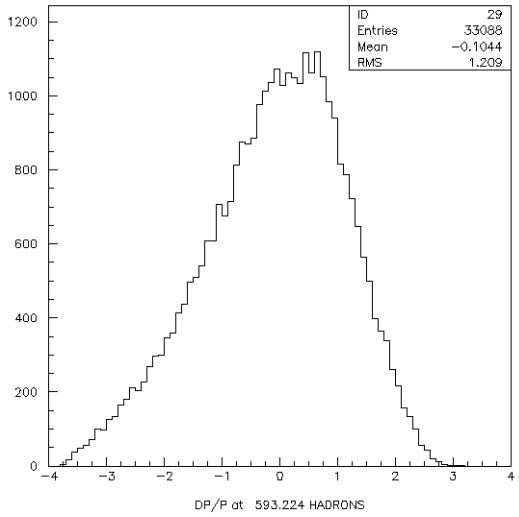

Figure 9: *The momentum spectrum of the beam delivered to the experiment*

In Figures 10 and 11 we show respectively the horizontal and vertical spot sizes and the angular distributions at the first RF cavity, RF1.

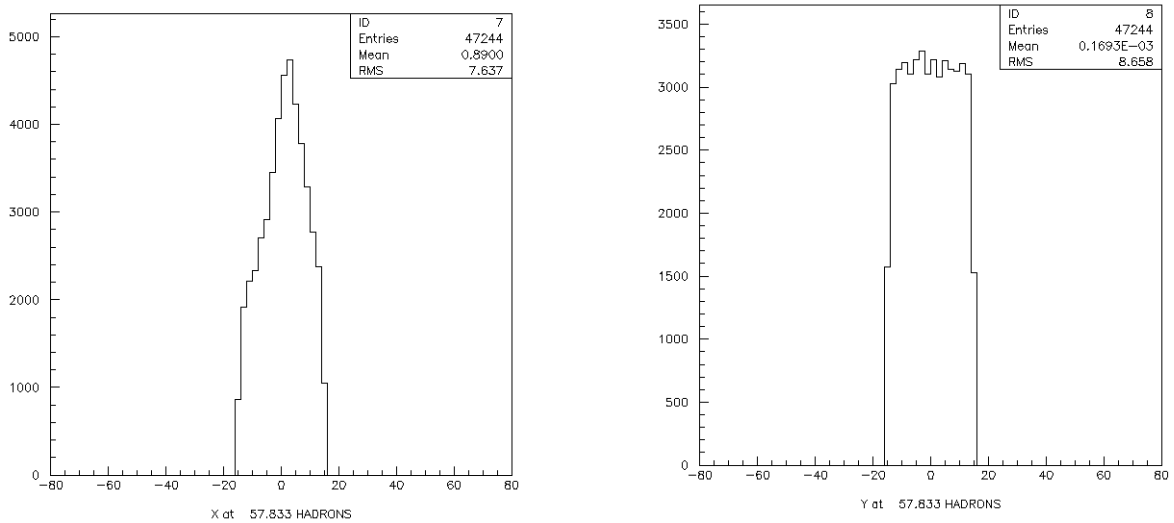

Figure 10: *The horizontal (left) and vertical (right) spot size at RF1*

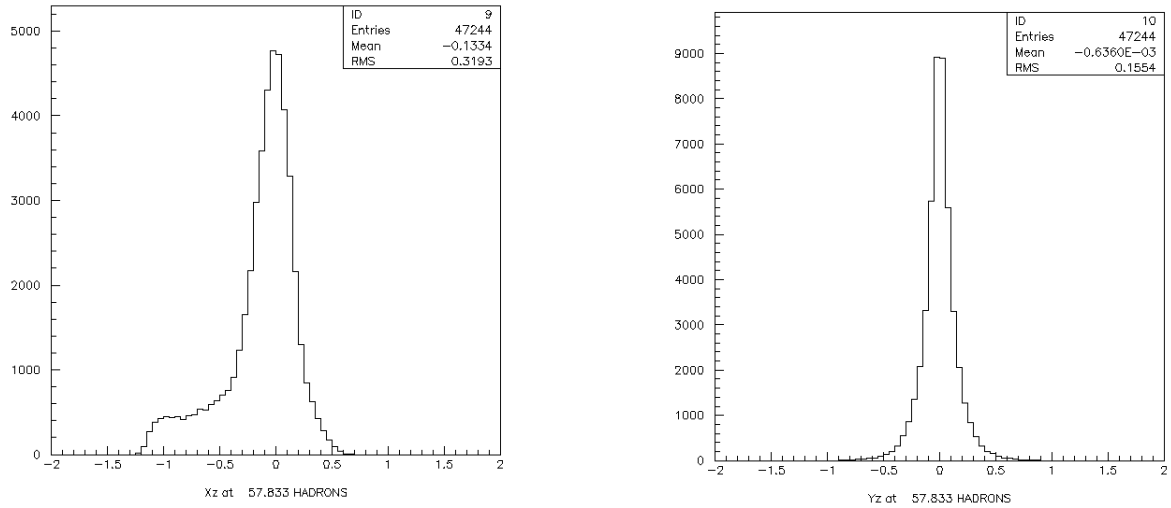

Figure 11: *The horizontal (left) and vertical (right) angular distributions at RF1*

In Figures 12 and 13 we show respectively the horizontal and vertical spot sizes and the angular distributions at the second RF cavity, RF2.

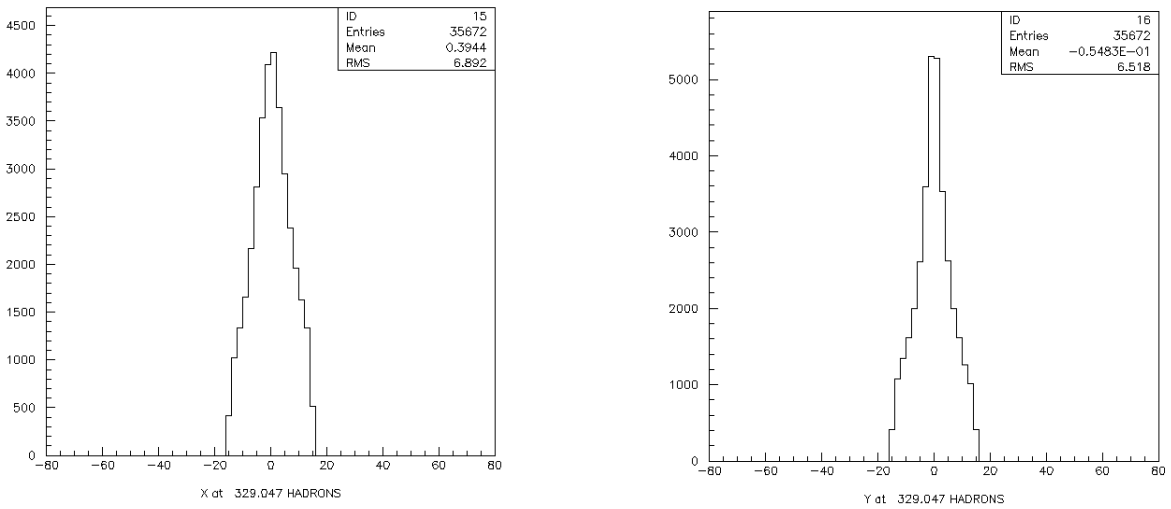

Figure 12: *The horizontal (left) and vertical (right) spot size at RF2*

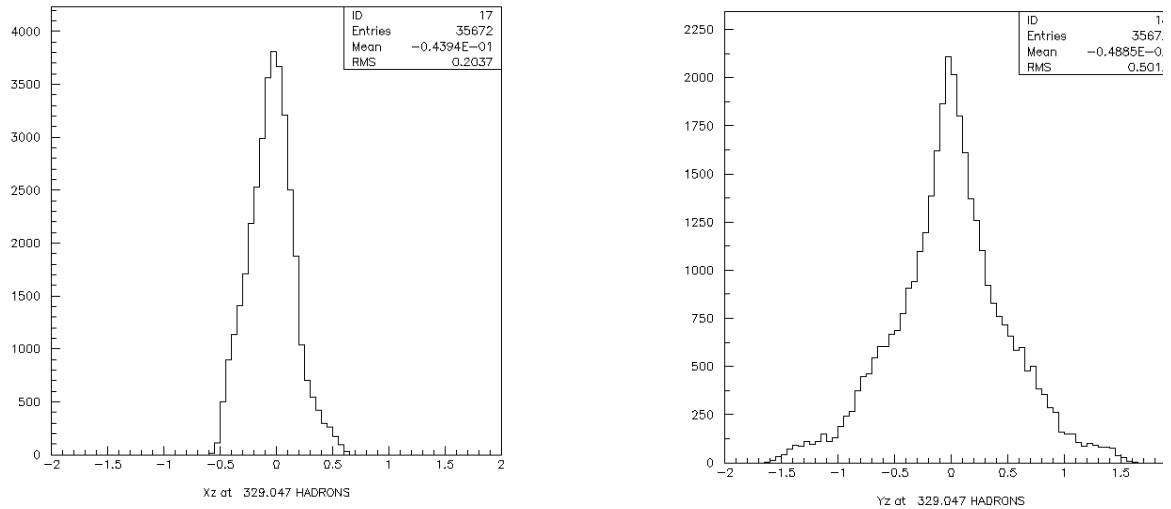

Figure 31: *The horizontal (left) and vertical (right) angular distributions at RF2*

The spot size of the (straight) beam at the p/π/e$^+$ collimator is shown in Figure 14.

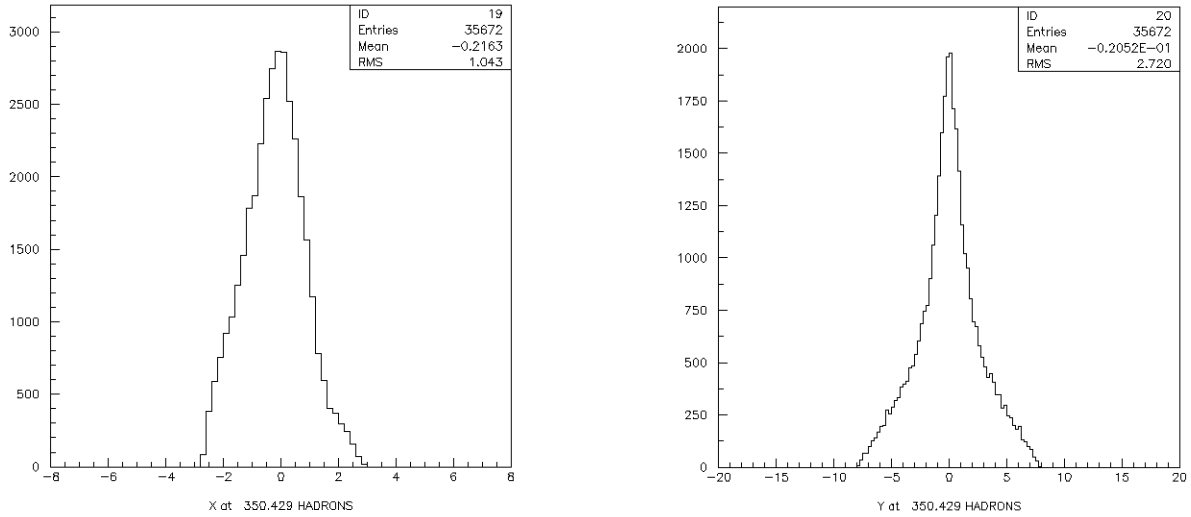

***Figure 14**: **T**he horizontal (left) and vertical(right) spot size at the* p/π/e$^+$ *collimator.*

This is a promising starting point for initial studies of the performance of the RF system.

Independent of the RF system, the kaon flux per proton suffers from decays and from the lower beam momentum. In Table 1 we show the different factors that affect the kaon flux per incident proton on the T10 target and the kaon content of the beam, before considering the impact of the RF system, with its inherent losses and impact on kaon content.

p_K (GeV/c)	Decays 105-165 m (present T10 position)	Decays 428-488 m (new T10 position)	% of K^+ at 135 m	% of K^+ at 458 m
75	**1.0**	0.564	**6.56%**	4.11%
60	0.829	**0.405**	6.04%	**3.35%**

***Table 1:** The impact of K^+ decays and lower beam momentum on kaon flux per incident proton on the T10 target and on the kaon content.*

From the table it is clear that kaon flux conservation is of prime importance. The main part of flux reduction by a factor of 2.5 is due to kaon decays. The purity decreases by a factor of about 2 before RF enrichment. The maximum increase of proton flux is a factor of 6 (to 2 10^{13} ppp), therefore the maximum gain in kaon decays is a factor of about 2.4. To reach a kaon fraction of the order of e.g. one third, the kaons must be enriched by a factor of 10.

5. The effects of the RF system on the optics

The RF system consists of two cavities, RF1 and RF2. RF1 gives a horizontal kick to the beam. A 3 m long cavity with 5 MeV/m kick gives a 15 MeV/c kick which corresponds to an angle of 0.25 mrad at 60 GeV/c. The second cavity should, at least approximately, cancel this kick (for at least one type of particle). In between the cavities, the central beam trajectory is affected by this kick. This effect was not yet included in the optics shown in Figure 8. In Figure 15 we show the optics from RF1 to RF2 and even up to the $p/\pi/e^+$ collimator, which gives in particular also the R_{12} term from RF1 to any beam element up to RF2 and the offset at the collimator. Details can be found in [6]. The largest excursions occur around Q17 and Q18. In Figure 16 we compare the maximum excursion with the physical aperture radius, as defined in Turtle (i.e. a circular chamber). In practice the aperture radius is usually 1 to 2 mm smaller due to the vacuum chamber thickness. In practice, for Q17 and Q18, one may insert 'marguerite shaped' vacuum chambers, which are more expensive to construct but provide a significantly larger horizontal aperture. The comparison for a few quadrupole type chambers is given in Table 2.

Quadrupole	**Round chamber**	**Marguerite chamber**
QNL	37.5	48
QTS	37.5	48
QWL	47.5	120
QNR	60	36

Table 2: *Comparison of apertures for round and marguerite type vacuum chambers.*

Q18 may be replaced by a QPL magnet, as the required GL allows it (12.6 T, to be compared to the maximum GL of 22 T for a QPL quadrupole). However, Q17 needs a GL of 32.2 T, which exceeds the maximum for a QPL. If necessary, it could be replaced by a new magnet with the same length as a QWL (2.948 m), but an aperture radius of 80 mm (instead of 50 mm for a QWL). The field at the pole tip is now 0.55 T, which can easily be increased to 0.9 T to provide a similar gradient in case of a larger aperture.

In conclusion, the beam transport through the delay line between the cavities should not induce significant additional losses. This remains to be validated by a full MADX simulation including the full transfer matrix, second order effects and the RF cavities themselves.

K12RFBEAM FOR NA62+ FRzom RF1 to RF2

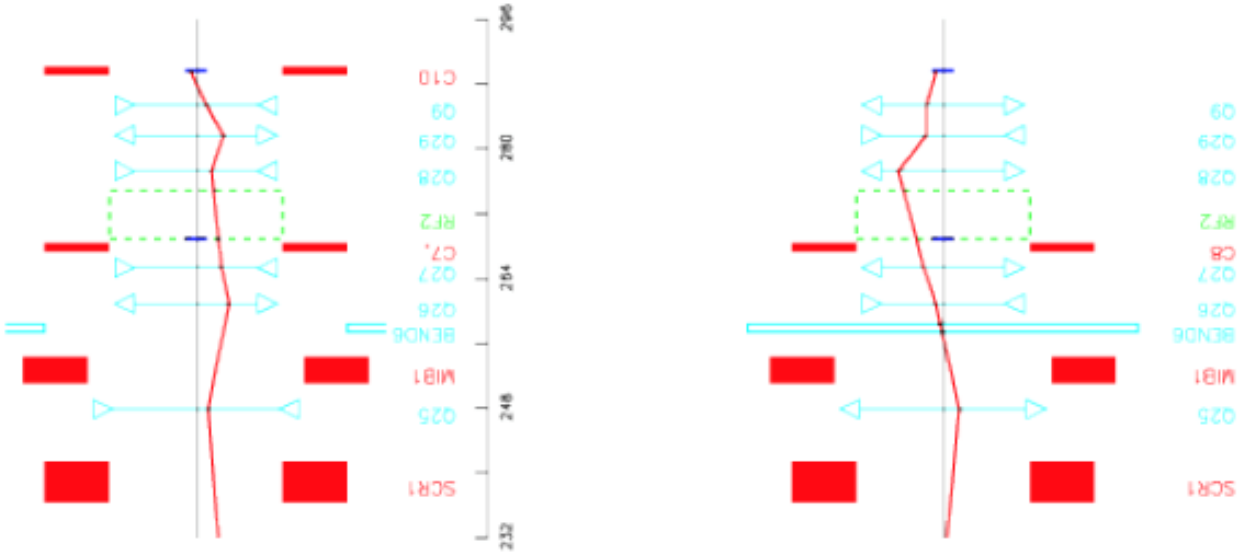

Figure 15: *The transfer matrix from RF1 up to RF2 and the p/π/e+ collimator*

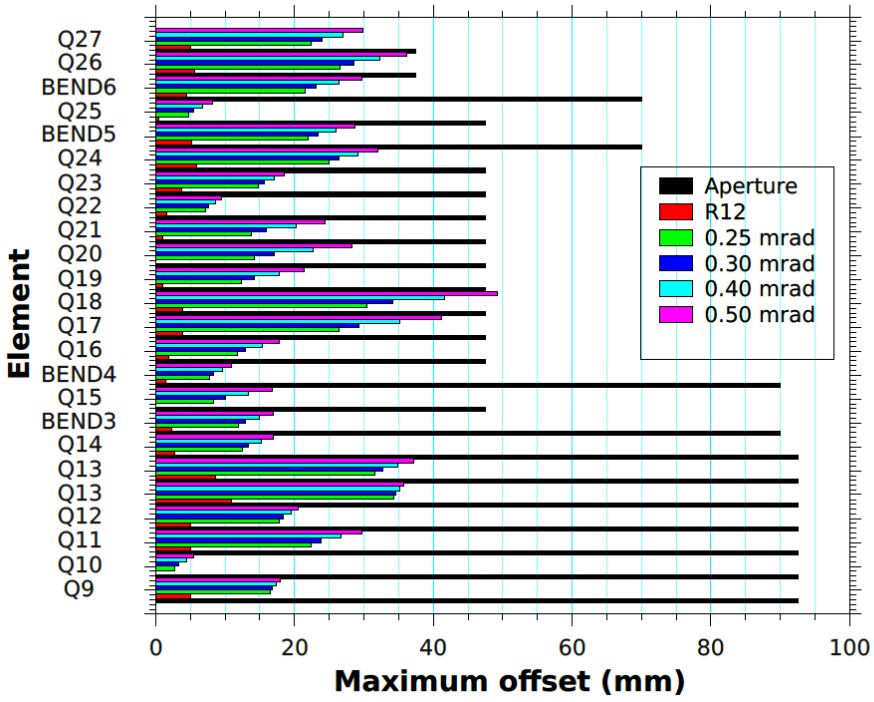

Figure 16: *The maximum excursion for different RF1 kicks compared to the beam acceptance. The physical acceptance is shown in black, the different colours correspond to different* p_t *kicks*

6. Assessment of the compact RF separator performance

Depending on the time of arrival of a particle at RF1, it will receive a horizontal deflection by an angle θ_{RF1} determined by the strength of the cavity, i.e. length times RF field. We are presently discussing maximum kicks between 0.25 and 0.5 mrad, but the real kick varies over the RF period according to a sine wave as a function of time. The optics between RF1 and RF2 ensures a one-to-one image of the RF1 beam at RF2 in the horizontal plane. The particles therefore have the same angle when they reach RF2. The RF2 cavity runs at the same frequency as RF1 and the phase is tuned to cancel the kick at RF1 for the kaons. Protons, pions and positrons have a different mass and therefore a different velocity. They will therefore arrive at a different phase with respect to the RF2 kick and the angle from RF1 will not be cancelled completely. The protons and pions will thus leave RF2 at a different angle and will be partly stopped in the p/π/e^+ collimator, which is located at 90° beam optics phase advance from RF2. The distance between the centres of the two cavities is 271.814 m and the speed of light is 2.99792458 m/s. The masses, velocities and travel times from RF1 to RF2 for the different particle types at 60 GeV/c are listed in Table 3.

Particle	Mass (GeV/c^2)	β = p/E	V = βc (m/s)	Travel time (ns)
π^+	0.13957062	0.9999973	299791646.90	906.67636
K^+	0.493677	0.9999662	299782310.67	906.70460
p	0.93827208	0.9998778	299755808.66	906.78476

Table 3: *Masses, velocities and travel times for the different particle species.*

The time and phase differences (assuming 5 GHz RF frequency) between K^+ and π^+ or protons are listed in Table 4.

Particle type	$t_{particle} - t_K$ (ns)	$\phi_{part} - \phi_K$ (°) for 5 GHz
π	0.0282370	50.827
p	0.0801535	144.294

Table 4: *Time and phase differences with respect to K^+ at RF2 for pions and protons, assuming a RF frequency of 5 GHz*

The kick after RF2 for maximum kick in RF1 is $(1-\cos\phi) \cdot \theta_{RF1}$, where ϕ is the phase difference at RF2, see Figure 17 for an illustration.

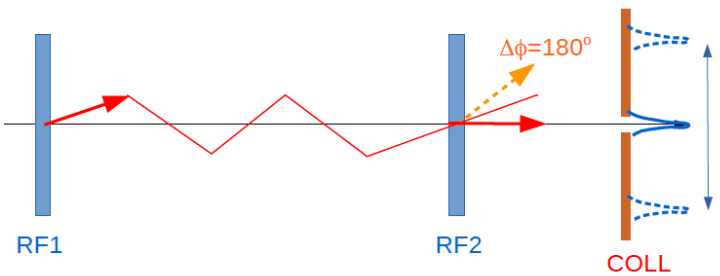

Figure 17: *Illustration of the kick dependence after the two cavities as a function of the phase difference with respect to the kaon phase. The red arrow corresponds to the kaon, the orange one to the maximum deflection for 180° phase difference ($\cos\phi = -1$)*

However, the phase at RF2 is different for each particle and then the total kick θ_{RF2} after RF2 is then

$$\theta_{RF2} = \theta_{RF1} \cdot \{\sin(\alpha(t)) - \sin(\alpha(t)+\phi)\},$$

where $\alpha(t)$ is the RF phase in the first cavity. This can be rewritten as

$$\theta_{RF2} = \theta_{RF1} \cdot \{\sin((\alpha(t)+\phi/2) - \phi/2) - \sin((\alpha(t)+\phi/2) + \phi/2)\}$$

and then

$$\theta_{RF2} = \theta_{RF1} \cdot \{\sin(\alpha(t)+\phi/2) \cdot \cos(\phi/2) - \sin(\alpha(t)+\phi/2) \cdot \cos(\phi/2) - \sin(\alpha(t)+\phi/2) \cdot \cos(\phi/2) - \sin(\alpha(t)+\phi/2) \cdot \cos(\phi/2)\}$$

hence

$$\theta_{RF2} = \theta_{RF1} \,.\, \cos(\alpha(t)+\phi/2) \cdot \sin(\phi/2).$$

The maximum net combined angular kick after RF1 and RF2 is therefore

$$\theta_{max} = 2\ \theta_{RF1} \cdot \sin(\phi/2)$$

(or $\theta_{max} = \theta_{RF1} \sqrt{2(1 - cos\phi)}$, which corresponds to $0.858 \cdot \theta_{RF1}$ for pions and $1.904 \cdot \theta_{RF1}$ for protons at nominal momentum. The kick follows the sine wave of the kick of the cavities, with a $\phi/2$ phase shift with respect to RF1.

The momentum dependence of the kaon phase is shown in Figure 18.

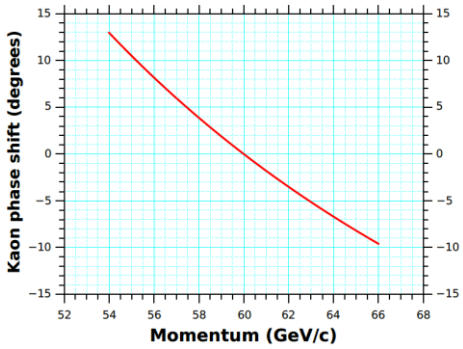

Figure 18: *The phase shift of K^+ as a function of particle momentum*

The variation of the phase difference between pions or protons and kaons is shown in Figure 19.

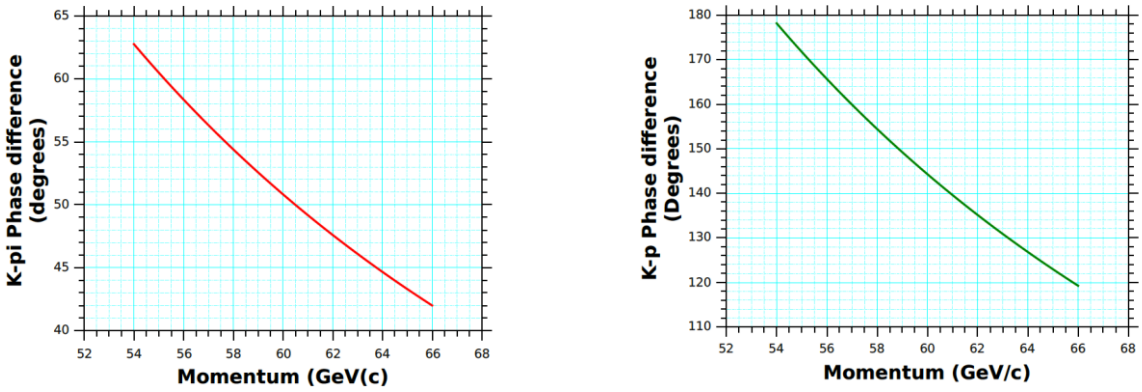

Figure 19: *The variation of phase difference between kaons and pions or protons with momentum*

A $\Delta p/p$ of 1.2% corresponds to a shift of the K^+ phase of about 2.2°, which is a small effect. The phase differences between kaons and pions or protons vary by similar amounts. It is of course very important that the frequencies of the two cavities are identical. This can be achieved by synchronising the RF drive via a master clock.

In Figure 20 we show the variation of the K-π and K-p phase difference with RF frequency at 60 GeV/c.

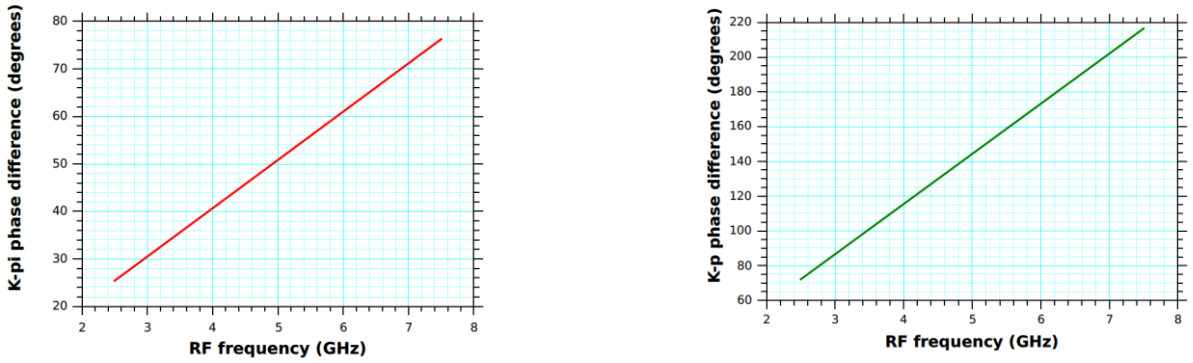

Figure 20: *The change of the phase differences between pions or protons with respect to kaons as a function of RF frequency for a 75 GeV/c beam*

It would require a huge increase of frequency to substantially increase the pion rejection. However, as shown in Figure 21, a small change of RF frequency allows fine tuning of the phase for kaons to cancel the RF1 kick precisely.

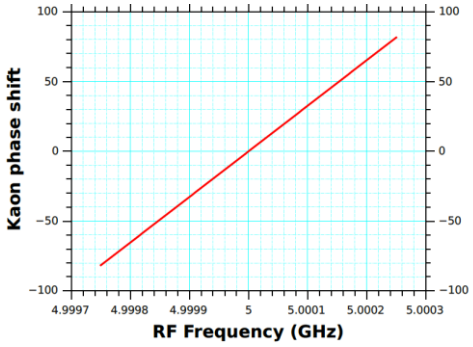

Figure 21: *The shift of kaon phase as a function of RF frequency*

The angular kicks of pions, kaons and protons at the exit of RF2 are shown as a function of the maximum kick strength in milliradians per cavity are shown in Figure 22. The optics from RF2 to the p/π/e^+ collimator gives an offset of 5 mm/mrad at this collimator and this offset is plotted in the right-hand plot of the figure.

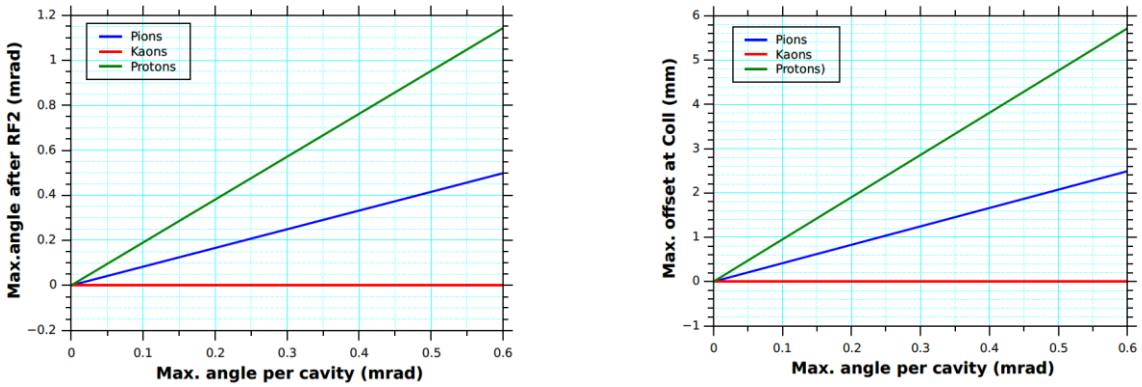

Figure 22: *The net angle for each particle type at the exit of RF2 and the offset at the p/π/e^+ collimator as a function of the kick strength per cavity.*

The beam profile of the unbent beam at the collimator has been shown in Figure 14. In Figure 23 we show the overall beam profile (no e^+), which has been constructed from the profile of Figure 14 overlaid with the same profile, but shifted by -2.15 mm and scaled by a factor 20 for the pions, and shifted by 4.76 mm and scaled by a factor 6.4 for the protons, more or less according to the expected beam composition and offsets. A possible collimator gap is indicated by the black lines in the figure.

However, the offset due to the RF kick follows a sine-wave according to the RF phase at the time of particle arrival. To estimate the transmission efficiency for the different particles, we have parameterised the efficiency as a function of the instantaneous offset with a gaussian, see Figure 24. The transmission is the fraction of the beam passing through the aperture.

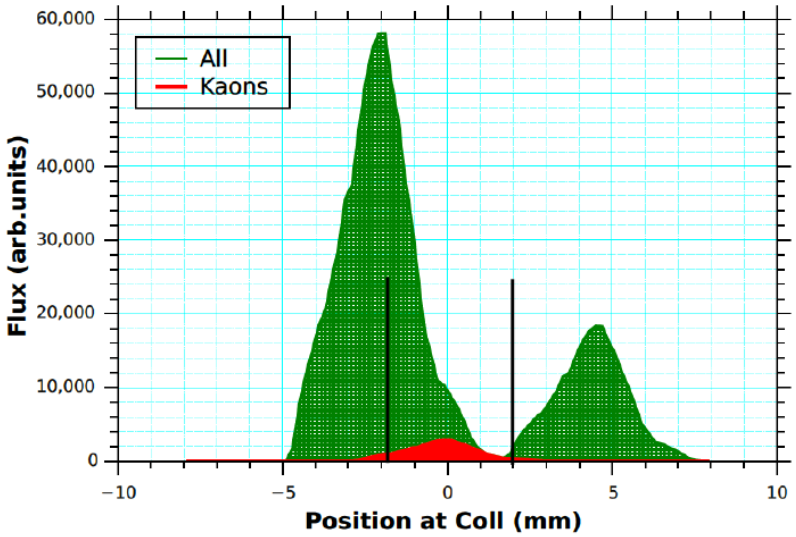

Figure 23: *The expected total beam profile incident on the p/π/e^+ collimator is shown in green and the kaon component in red. The two black lines show a possible collimator setting. The offsets correspond roughly to 0.5 mrad maximum kicks per cavity.*

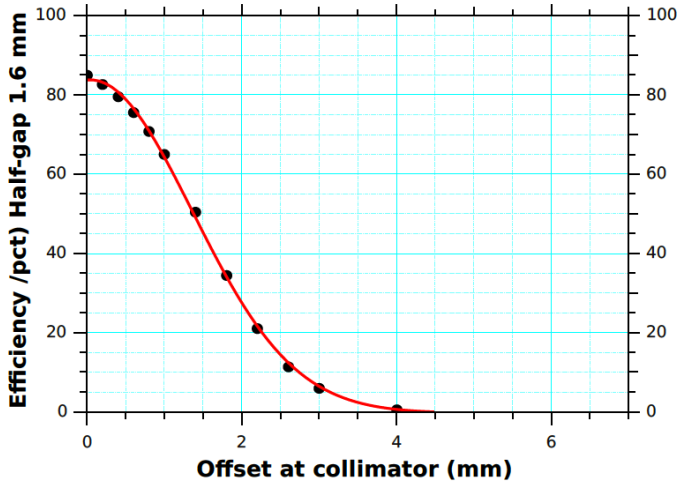

Figure 24: *The transmission as a function of beam offset at the collimator as fitted with a gaussian*

The parameters of the fit are: A = 277.19, w = 2.6305, x_c=0.045, y_o = -0.2914, where the gaussian function g(x) is defined as

$$g(x) = y_o + A\frac{\sqrt{2/\pi}}{w}\, x^{-2((x-x_o)/w)^2}$$

The fit is very satisfactory. We use this function to calculate the efficiency versus time as

$$\varepsilon(t) = g(k(t))$$

where the instantaneous offset at the collimator k(t) is

$$k(t) = |k_{max} sin(t)|$$

where k_{max} is the offset at the time of maximum kick.

We then average ε(t) over a half wavelength (the second half of the wavelength has a negative phase, but the efficiency drop depends on the absolute value of the offset k(t)). The efficiency as a function of time is shown in Figure 25 for pions (k_{max} = 2.15 mm) and protons (k_{max} = 4.76 mm), corresponding to a 0.5 mrad maximum kick per cavity. The global efficiency for pions is 49.3%, for protons 19.9%.

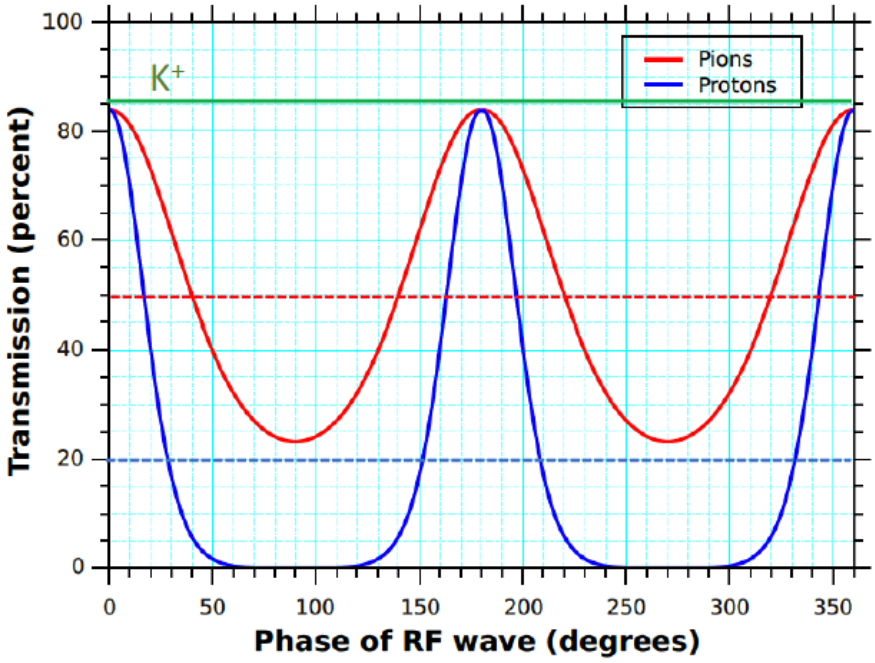

Figure 25: *The transmission efficiency through the collimator as a function of time over a RF wavelength for pions (in red) and for protons (in blue). The green line indicates the efficiency for kaons and the dotted lines the average transmission efficiency per species.*

The average estimated transmission efficiencies for the different particle types are shown in Table 5. Figure 26 shows the average transmission over a RF cycle as a function of the phase difference with respect to kaons.

Particle type	Transmission efficiency (%)
π^+	49.3
K^+	85.1
p	19.9

Table 5: *The estimated average transmission efficiencies per particle type*

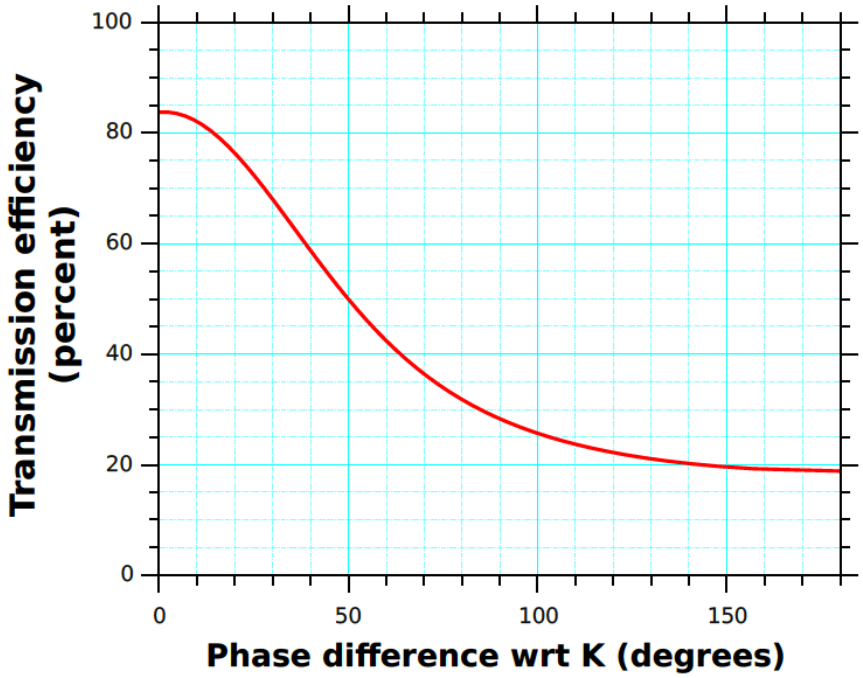

Figure 26: *The average transmission over the time of a RF cycle versus the phase difference between a particle type and a kaon*

The resulting kaon purity is only 5.1%, less than for a (much shorter!) unseparated beam. Clearly this RF system cannot compensate for the decays of the kaons. This is because the phase difference between kaons and pions is insufficient for useful separation.

A sharper focusing at the collimator does not help, as the effect of the kick leads to proportionally smaller offset at the collimator. E.g. with a magnification of 0.3 instead of 1, the offset per milliradian at RF2 decreases from 5 to 1.5 mm/mrad.

7. Other possible options

The result is not satisfactory for the moment, in particular in view of the very large investment needed to install such a beam line. An increase of the RF frequency would surely be beneficial for the kaon enrichment. A further decrease of beam momentum would help the RF phase difference but decrease further the initial kaon fraction and require a significant increase of the gas pressure in the KTAG (and hence the scattering and interaction rate in the gas and the windows). Lengthening the beam would also help for the RF enrichment factor, but the increase of the fraction of kaons that decay before reaching the experiment would quickly render the exercise meaningless. In the following paragraphs we have a somewhat closer first look at these options.

7.1 The 'standard' approach to RF separation

In the 'standard approach' to RF separated kaon beams the phase difference between pions and protons is set to 360 degrees and the RF phase tuned such that both pions and protons are dumped in a collimator. In that case the kaons have a phase difference of -102^o with respect to pions and protons. In our case the maximum offset between the kaons and the pion+proton beam would be 0.5 mr $\cdot$ 2 $\cdot$ sin(51^o) $\cdot$ 5 mm/mr = 3.89 mm. From Figure 24, one sees that the transmission for pions and protons would below 3%, which is of course quite good for kaon purity. However, in this case the kaons are moved over the collimator where the pions and protons are stopped and a fraction will be lost. Alternatively, the RF phase is set for the kaons to go straight and from Figure 26 one sees that the π/p transmission is about 30%. However, the distance between the two cavities must be 501.4 m for 60 GeV/c and an RF frequency of 5 GHz. To this one must add about 210 m for the front-end and the beam from RF2 to the start of the decay volume of NA62. The total beam length increases by about 230 m. The effect is a further decrease of the kaon flux by a factor of 1.66 (1.4 times NA62 rate) and the natural K^+ component before RF enrichment in the beam is reduced to about 2%. The kaon component at the end would remain at the ≈ 6% level.

This scheme also has important impacts on the RP issues and their consequences for civil engineering and shielding. The target would move to a position around 286 m from the T4 target, i.e. at the present location of P42-Coll1+2. This is a narrow tunnel section with small separation from the TT81 tunnel towards EHN1. The front-end would become similar to the present NA62 one (with an achromat, horizontal or vertical), but the replacement of the present Bend7 (with dispersion recombination) would remain problematic for the beam optics.

7.2 Increasing the length a bit

Instead of going all the way towards the solution suggested in section 7.1, one could use the NA62 front-end followed by a delay line up to the present BEND7 location. Such a delay line must be of similar length as the present sections between bends, i.e. of the order of 100 m. The beam length would thus increase by about 120 metres and the kaon flux would only be reduced by a factor 1.3 instead of 1.66. However, the RP problems remain similar. The distance between cavities would increase to about 370 m. At 60 GeV/c and a RF frequency of 5 GHz, the phase difference between kaons and pions or protons would become 69 or 196^o, respectively. The protons would essentially be removed and the pions reduced by a factor of about 3 (maximum offset 2.8 mm), if all other conditions remain unchanged. This option seems less promising than the one of section 7.1, as the beam remains strongly pion dominated (kaon fraction remains well below 20%).

7.3 Decreasing the beam momentum

A further decrease of beam momentum would lead to a better performance of the RF system, but must be offset to a further increase of the number of kaon decays and the need for higher gas pressures in the KTAG Cerenkov counter. At 50 GeV/c the π-K phase difference is -73.2° and the p-K phase difference 207.8°. The offsets at the collimator are then 2.98, respectively 4.85 mm. The pion flux would be reduced by a factor of about 3.3, ≈ 80% of the protons would be removed. A momentum of 45 GeV/c or lower would be required to reject 90% of the pions. In Figure 27 we show the decrease of the number of kaons decays over 60 metres starting at 428 metres from the target as a function of momentum. The number of decays at 45 GeV/c is 55% of the rate at 60 GeV/c and 40% of the rate at 75 GeV/c.

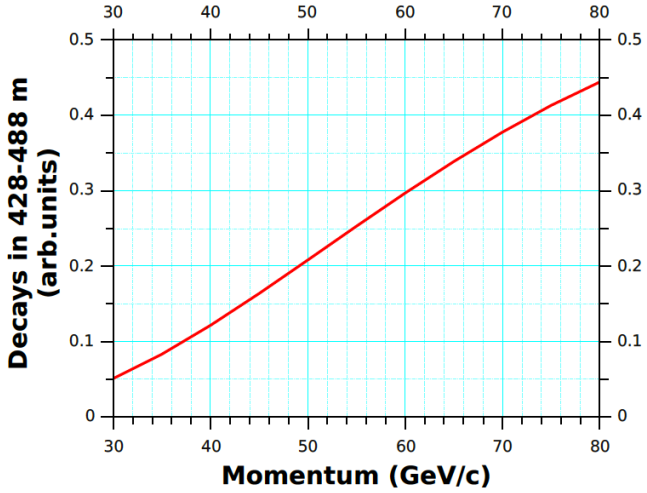

Figure 27: *The number of kaon decays between 428 and 488 from the target as a function of momentum*

7.4 Increase of RF frequency

Theoretically a higher RF frequency would solve the problem if it would be technically possible to operate such a cavity at the required duty cycle, with a similar RF kick and the same iris size. From Figure 26 we see that a phase difference well above 90 degrees with respect to the kaons is needed for both pions and protons, if their rate should be decreased by a factor of around 5. This requires the phase difference between pions (and protons) and kaons to be larger than 90°. The frequency of the cavities must be at least 9 GHz. Possibly liquid Nitrogen cooled copper cavities can be operated with an RF kick of 5 MV/m at frequencies up to 12 GHz.

However, the iris diameter reduces to probably 18 to 20 mm. Considering the sagitta for the deflected particles, this means that the useful aperture reduces to about 17 mm diameter. Reducing the beam size at the cavities would increase the angular spread and therefore reduce again the RF separation. Therefore, one would collimate the beam outside this aperture away. The rate would then reduce by a factor 2.8 to 0.7 times the present nominal NA62 intensity. The spot at the proton/pion dump reduces only slightly, so one would keep the same collimator slit. The intensity reduction would be prohibitive.

7.5 Adding more cavities

Longer or more cavities allow a larger angular kick and therefore an increase of the offset at the collimator. However, a larger angular kick becomes problematic for the acceptance of the delay line. This may be solved by replacing some quadrupoles by large aperture and still strong super-conducting quadrupoles.

Also, the displacement at the end of the cavity system due to its kick becomes large. It is given by θ. $L_{cav}/2$ =where θ is equal to the product of L_{cav} and the RF field (MV/m). For 3 m of cavities, θ = 0.25 mrad and $L_{cav}/2$ = 1.5 m, hence the maximum kick is ±1.5 x 0.25 = ±0.375 mm, small compared to the iris size (R = 15 mm). For 6 m cavities, this becomes ±3 x 0.5 = ±1.5 mm. For 12 m of cavities it becomes ±6 mm, which eats very significantly in the acceptance and therefore into the beam flux.

8. Conclusion and outlook

The heart of the problem lies in the fact that the pions are the dominating component in the beam and their phase difference with respect to kaons is too small to give a sufficient separation. The maximum total kick for the pions is smaller than the maximum kick of a set of cavities and the average kick is even much smaller, leading to a limited reduction factor. Even the protons are not yet fully separated and their rate is only reduced by a factor of 5. A larger transverse kick would also help, but it becomes very difficult then to transport the beam along the delay line without using superconducting quadrupoles in that section. The beam optics can be designed to transport the beam with good acceptance, even in the presence of the RF kick (note: the matching to the NA62 detectors remains to be studied).

The most promising solution remains therefore an increase of RF frequency, if that can still remain compatible with the high duty cycle typically used and also required in the North Area. And a decrease of iris size would also reduce the kaon rate.

Unfortunately, the possibilities for increasing the performance with respect to a non-separated beam are not convincing and the cost would be very significant.

In cases where a lower kaon intensity can be accepted, the distance between cavities can be increased and in that case the phase differences can become more favourable. Possibly also the emittance of the beam can then be reduced, thus allowing better angular separation between the wanted and unwanted particles In such cases it is not excluded that a satisfactory solution can be found, but this requires a dedicated study for the experiment and beam line in question.

Acknowlegement

The authors thank Gianluigi Arduini and Rhodri Jones for careful reading of the manuscript.

References

1. E.Cortina Gil et al. (the NA62 collaboration), The beam and detector of the NA62 experiment at CERN, 2017 JINST 12 P05025
2. A. Buras et al., $K^+ \rightarrow \pi^+ \nu\bar{\nu}$ and $K_L \rightarrow \pi^o \nu\bar{\nu}$ in the Standard Model: status and perspectives, JHEP 11 (2015) 033
3. G.Anelli et al., Proposal to measure the Rare Decay $K^+ \rightarrow \pi^+ \nu\bar{\nu}$ at the CERN SPS, SPSC-P-326, 2005.
4. C.Adolphsen et al. Design of the ILC Crab Cavity System, EUROTeV Report-2007-010, SLAC-PUB-12751
5. L.Gatignon, Design and Tuning of Secondary Beamlines in the CERN North and East Areas CERN-ACC-Note-2020-0043, http://gatignon.web.cern.ch/gatignon/CERN-ACC-NOTE-2020-0043.pdf
6. http://cern.ch/gatignon/k12rfbeam-html
7. C.Iselin, Decay Turtle, a Computer Program for Simulating Charged Particle Beam Transport Systems, including Decay Calculations, CERN 74-2

APPENDIX A: ASYMMETRIC SPLITTING OF BENDS WITH DISPERSION RECOMBINATION

In several locations we have a net deflection of the beam with the necessity to recombine the dispersion. The basic layout is shown in Figure A.1 (same as Figure 3 in the main text).

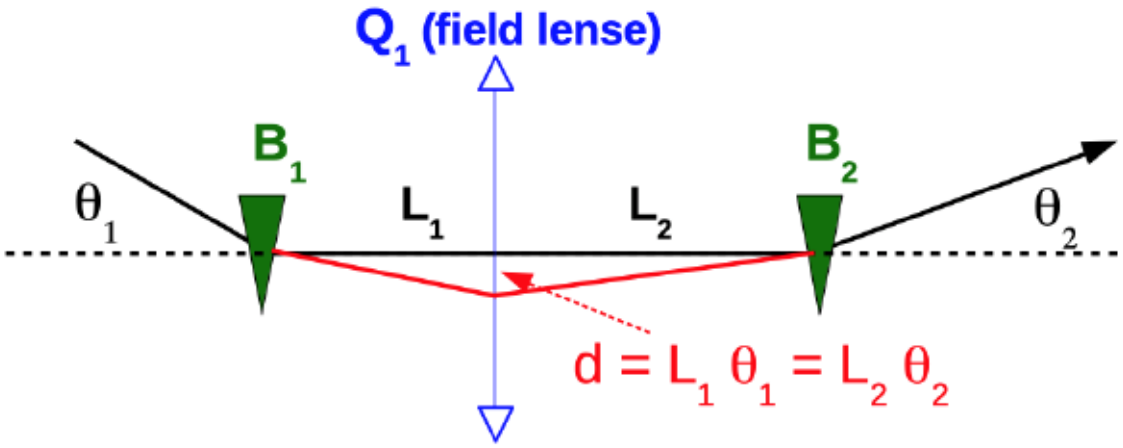

Figure 6: *Explanation of how dispersion can be recombined by focusing in between two dipoles. Note that the two angles may be different.*

The quadrupole is positioned according to the rule

$$\frac{L_1}{L_2} = \frac{\theta_2}{\theta_1}$$

The strength (integrated gradient GL) of the quadrupole is given by the focal distance f = 3.3357 p/f, which varies with $L = L_1 + L_2$ roughly as $f \approx L/4$ (thin lens approximation and symmetric system). Often a symmetric layout with $L_1 = L_2$ is used, but different L_1 and L_2 values can be an advantage, like in our application. Let us illustrate our situation with the last vertical bend (the replacement of BENDs 10 and 12 of the present P42 beam line).

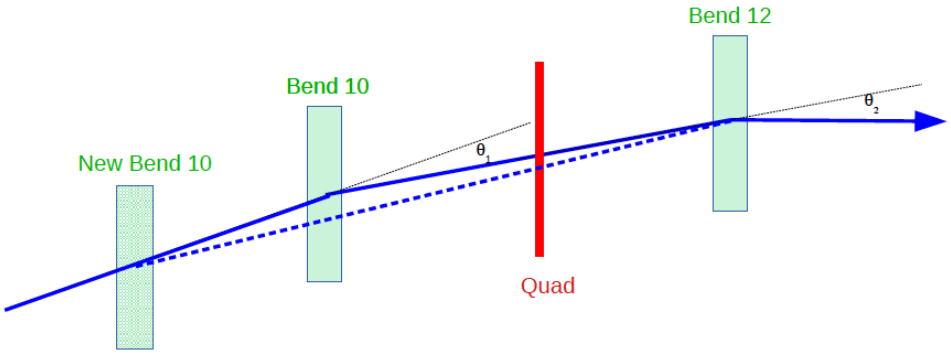

Figure A.2: *The layout of the replacement of BENDs 10 1and 12 in the new RF separated beam.*

In the picture the solid blue line shows the symmetric situation, the dashed line am asymmetric one, where the overall distance $L = L_1+L_2$ between the bends is increased, whereas the BEND12 position is maintained. In the case of the symmetric layout in this example $\theta_1 = \theta_2 \stackrel{def}{=} \theta_o = 4.824$ mrad and $L_1 = L_2 \stackrel{def}{=} L_o = 10$ m, hence $L = 2 \cdot L_o = 20$ m. In case θ_2 is changed, $\theta_1 = 2\,\theta_o - \theta_2$ and by intersecting the dashed blue line with the incident beam trajectory one finds that L_1 becomes $L_1 = L_o + L \cdot (\theta_2 - \theta_o) / (2\,\theta_o - \theta_2)$ and L becomes larger by a factor θ_o / θ_1. L_2 remains unchanged. The variation of the different lengths with θ_2 is shown in Figure A.3

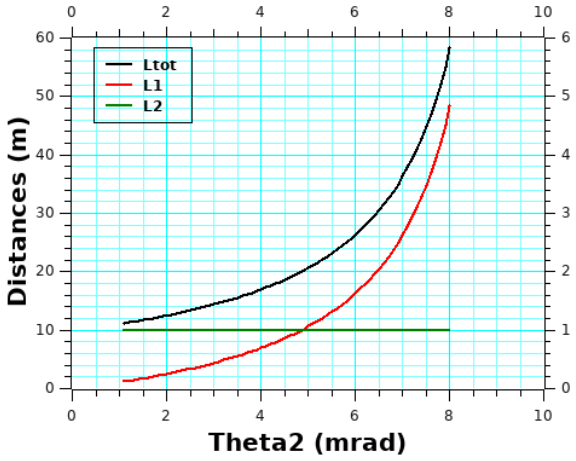

Figure A.3: *The variation of L_1, L_2 and L as a function of θ_2..*

The focal distance of the quadrupole to recombine dispersion as a function of θ_2 is shown in Figure A.4.

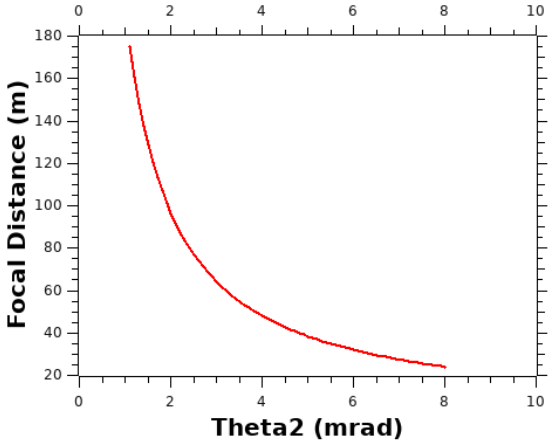

Figure A.4: *The focal distance of the quadrupole for dispersion recombination as a function of θ_2.*

This relates to an integrated gradient as a function of θ_2 as shown in Figure A.5. This calculation is based on thin lens approximation, where all the gradient is used in a position where it is most effective. A real quadrupole (QWL type) has a length of 2.948 m and its strength is used less efficiently. A real calculation with transport gives a slightly larger GL value (just over 10% more).

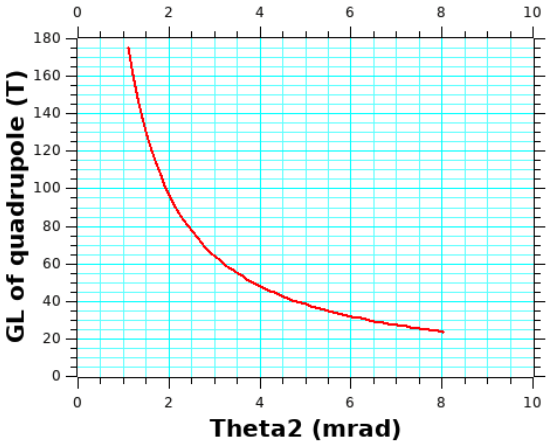

Figure A.5: *The GL of the quadrupole as a function of θ_2.*

APPENDIX B: TRANSPORT LISTINGS

K12RFBEAM - RF SEPARATED K+ BEAM FOR NA62+ TRANSPORT RUN12/12/20

POSITION METERS	TYPE		STRENGTH T*M,T/M*M T/M**2*M	HORIZONTAL R11 MM/MM	R12 MM/MR	R21 MR/MM	R22 MR/MR	VERTICAL R33 MM/MM	R34 MM/MR	R43 MR/MM	R44 MR/MR	DISPERSION R16 MM/PC	R26 MR/PC	R36 MM/PC	R46 MR/PC
0.000	3	T12		1.000	0.000	0.000	1.000	1.000	0.000	0.000	1.000	0.000	0.000	0.000	0.000
3.750	3			1.000	3.750	0.000	1.000	1.000	3.750	0.000	1.000	0.000	0.000	0.000	0.000
6.740	5	Q1	-32.1128	1.250	7.921	0.174	1.901	0.770	5.642	-0.148	0.215	0.000	0.000	0.000	0.000
7.180	3			1.326	8.757	0.174	1.901	0.704	5.737	-0.148	0.215	0.000	0.000	0.000	0.000
10.170	5	Q2	72.6595	1.099	9.128	-0.311	-1.675	0.596	9.908	0.069	2.823	0.000	0.000	0.000	0.000
10.825	3			0.895	8.031	-0.311	-1.675	0.641	11.757	0.069	2.823	0.000	0.000	0.000	0.000
10.825	3	MDXV		0.895	8.031	-0.311	-1.675	0.641	11.757	0.069	2.823	0.000	0.000	0.000	0.000
11.380	3			0.723	7.101	-0.311	-1.675	0.679	13.324	0.069	2.823	0.000	0.000	0.000	0.000
14.370	5	QN3	-50.9306	-0.038	4.308	-0.229	-0.309	0.618	15.978	-0.107	-1.161	0.000	0.000	0.000	0.000
14.970	3			-0.176	4.123	-0.229	-0.309	0.553	15.282	-0.107	-1.161	0.000	0.000	0.000	0.000
18.570	4	B1	5.4038	-1.001	3.007	-0.229	-0.310	0.166	11.101	-0.107	-1.161	0.486	0.270	0.000	0.000
21.600	3			-1.696	2.068	-0.229	-0.310	-0.159	7.582	-0.107	-1.161	1.304	0.270	0.000	0.000
23.200	3	dmp1		-2.063	1.572	-0.229	-0.310	-0.331	5.724	-0.107	-1.161	1.736	0.270	0.000	0.000
23.210	3			-2.065	1.569	-0.229	-0.310	-0.332	5.713	-0.107	-1.161	1.739	0.270	0.000	0.000
24.810	3	dmp		-2.432	1.072	-0.229	-0.310	-0.504	3.855	-0.107	-1.161	2.171	0.270	0.000	0.000
24.890	3			-2.450	1.048	-0.229	-0.310	-0.513	3.762	-0.107	-1.161	2.192	0.270	0.000	0.000
25.190	3			-2.519	0.955	-0.229	-0.310	-0.545	3.413	-0.107	-1.161	2.273	0.270	0.000	0.000
25.690	3			-2.634	0.800	-0.229	-0.310	-0.599	2.833	-0.107	-1.161	2.408	0.270	0.000	0.000
26.190	3			-2.748	0.644	-0.229	-0.310	-0.653	2.252	-0.107	-1.161	2.543	0.270	0.000	0.000
26.390	3			-2.794	0.582	-0.229	-0.310	-0.674	2.020	-0.107	-1.161	2.597	0.270	0.000	0.000
26.430	3	CONV		-2.803	0.570	-0.229	-0.310	-0.678	1.973	-0.107	-1.161	2.608	0.270	0.000	0.000
26.510	3			-2.822	0.545	-0.229	-0.310	-0.687	1.881	-0.107	-1.161	2.630	0.270	0.000	0.000
26.721	3			-2.870	0.480	-0.229	-0.310	-0.710	1.636	-0.107	-1.161	2.686	0.270	0.000	0.000
29.669	5	Q4	38.3145	-2.712	-0.480	0.332	-0.310	-1.267	-1.635	-0.288	-1.161	2.686	-0.270	0.000	0.000
29.940	3			-2.622	-0.564	0.332	-0.310	-1.345	-1.950	-0.288	-1.161	2.613	-0.270	0.000	0.000
30.440	3	COLL		-2.456	-0.719	0.332	-0.310	-1.489	-2.531	-0.288	-1.161	2.478	-0.270	0.000	0.000
30.940	3	XCHV		-2.290	-0.874	0.332	-0.310	-1.634	-3.111	-0.288	-1.161	2.343	-0.270	0.000	0.000
37.820	3			-0.008	-3.007	0.332	-0.310	-3.617	-11.101	-0.288	-1.161	0.486	-0.270	0.000	0.000
41.420	4	B2	5.4037	1.186	-4.123	0.332	-0.309	-4.655	-15.282	-0.288	-1.161	0.000	-0.000	0.000	0.000
41.715	3			1.283	-4.214	0.332	-0.309	-4.740	-15.624	-0.288	-1.161	0.000	-0.000	0.000	0.000
42.053	3			1.395	-4.318	0.332	-0.309	-4.837	-16.017	-0.288	-1.161	0.000	-0.000	0.000	0.000
45.043	5	Q5	-61.8377	3.242	-7.546	0.997	-2.013	-3.505	-12.132	1.110	3.556	0.000	0.000	0.000	0.000
46.483	3			4.679	-10.444	0.997	-2.013	-1.907	-7.011	1.110	3.556	0.000	0.000	0.000	0.000
49.473	5	Q6	64.5831	5.123	-10.895	-0.725	1.736	0.975	1.753	0.970	2.770	0.000	-0.000	0.000	0.000
50.913	3			4.079	-8.394	-0.725	1.736	2.373	5.742	0.970	2.770	0.000	-0.000	0.000	0.000
53.903	5	Q7	-42.0617	3.029	-5.420	-0.015	0.356	4.273	11.473	0.233	0.860	-0.000	-0.000	0.000	0.000
54.343	3			3.022	-5.263	-0.015	0.356	4.375	11.851	0.233	0.860	-0.000	-0.000	0.000	0.000
55.833	5	Q8	-14.0164	3.159	-5.000	0.200	-0.000	4.490	12.497	-0.080	-0.000	-0.000	-0.000	0.000	0.000
57.833	3			3.559	-5.000	0.200	-0.000	4.330	12.497	-0.080	-0.000	-0.000	-0.000	0.000	0.000
63.833	3	RF1		4.759	-5.000	0.200	-0.000	3.850	12.497	-0.080	-0.000	-0.000	-0.000	0.000	0.000
65.833	3			5.159	-5.000	0.200	-0.000	3.690	12.497	-0.080	-0.000	-0.000	-0.000	0.000	0.000
67.833	5	Q9	18.7788	5.070	-4.538	-0.288	0.455	3.877	13.689	0.270	1.210	-0.000	0.000	0.000	0.000
76.833	3			2.482	-0.447	-0.288	0.455	6.303	24.575	0.270	1.210	-0.000	0.000	0.000	0.000
78.833	5	Q10	-21.5129	2.158	0.447	-0.043	0.455	6.157	24.314	-0.412	-1.466	-0.000	-0.000	0.000	0.000
87.833	3			1.775	4.538	-0.043	0.455	2.446	11.120	-0.412	-1.466	-0.000	-0.000	0.000	0.000
89.833	5	Q11	18.7788	1.529	5.000	-0.200	0.000	1.828	9.155	-0.215	-0.529	-0.000	0.000	0.000	0.000
106.113	3			-1.727	5.000	-0.200	0.000	-1.671	0.536	-0.215	-0.529	-0.000	0.000	0.000	0.000
108.113	5	Q12	-12.5930	-2.246	5.318	-0.324	0.321	-1.988	-0.534	-0.099	-0.529	-0.000	0.000	0.000	0.000
124.536	3			-7.562	10.594	-0.324	0.321	-3.607	-9.230	-0.099	-0.529	0.000	0.000	0.000	0.000
126.536	5	Q13	10.8180	-7.792	10.657	0.095	-0.258	-4.005	-10.812	-0.302	-1.066	0.000	0.000	0.000	0.000
142.959	3			-6.231	6.415	0.095	-0.258	-8.973	-28.324	-0.302	-1.066	0.000	0.000	0.000	0.000
144.959	5	Q12	-12.5930	-6.434	6.295	-0.299	0.137	-9.007	-28.648	0.269	0.745	0.000	0.000	0.000	0.000
161.382	3			-11.349	8.552	-0.299	0.137	-4.586	-16.411	0.269	0.745	0.000	0.000	0.000	0.000
163.382	5	Q13	10.8180	-11.329	8.364	0.319	-0.324	-4.288	-15.789	0.031	-0.117	0.000	-0.000	0.000	0.000
179.805	3			-6.087	3.044	0.319	-0.324	-3.772	-17.717	0.031	-0.117	0.000	-0.000	0.000	0.000
181.805	5	Q14	-12.5930	-5.822	2.576	-0.052	-0.149	-3.475	-16.844	0.262	0.981	0.000	0.000	0.000	0.000
183.001	3			-5.883	2.398	-0.052	-0.149	-3.162	-15.670	0.262	0.981	0.000	0.000	0.000	0.000
184.001	4	B3	0.6574	-5.935	2.249	-0.052	-0.149	-2.900	-14.688	0.262	0.981	0.016	0.033	0.000	0.000
197.554	3			-6.633	0.230	-0.052	-0.149	0.649	-1.387	0.262	0.981	0.462	0.033	0.000	0.000
200.502	5	Q15	35.7888	-5.099	-0.230	1.046	-0.149	1.669	1.386	0.460	0.981	0.434	-0.051	0.000	0.000
208.528	3			3.297	-1.426	1.046	-0.149	5.365	9.262	0.460	0.981	0.025	-0.051	0.000	0.000
209.528	4	B4	1.0207	4.343	-1.574	1.046	-0.149	5.825	10.244	0.460	0.981	-0.000	0.000	0.000	0.000
210.052	3			4.891	-1.653	1.046	-0.149	6.067	10.758	0.460	0.981	-0.000	0.000	0.000	0.000
213.000	5	Q16	-41.5851	9.876	-2.670	2.506	-0.576	5.525	10.235	-0.809	-1.318	-0.000	0.000	0.000	0.000
213.582	3			11.334	-3.006	2.506	-0.576	5.054	9.467	-0.809	-1.318	-0.000	0.000	0.000	0.000
216.530	5	Q17	32.1279	15.576	-3.891	0.257	0.000	3.719	7.598	-0.132	-0.000	-0.000	0.000	0.000	0.000
225.441	3			17.866	-3.891	0.257	0.000	2.546	7.598	-0.132	-0.000	0.000	0.000	0.000	0.000
228.389	5	Q18	12.5069	16.981	-3.538	-0.849	0.236	2.384	8.308	0.020	0.489	0.000	0.000	0.000	0.000
237.301	3			9.416	-1.437	-0.849	0.236	2.563	12.670	0.020	0.489	0.001	0.000	0.000	0.000
240.249	5	Q19	-25.4771	8.577	-0.976	0.262	0.087	2.153	11.721	-0.290	-1.113	0.001	0.000	0.000	0.000
249.160	3			10.911	-0.203	0.262	0.087	-0.430	1.799	-0.290	-1.113	0.002	0.000	0.000	0.000
252.108	5	Q20	10.1773	10.856	0.062	-0.299	0.090	-1.338	-1.430	-0.334	-1.104	0.002	0.000	0.000	0.000
261.020	3			8.196	0.868	-0.299	0.090	-4.317	-11.269	-0.334	-1.104	0.002	0.000	0.000	0.000
263.968	5	Q21	8.1070	6.848	1.078	-0.606	0.051	-5.583	-15.269	-0.533	-1.636	0.002	-0.000	0.000	0.000
272.879	3			1.445	1.529	-0.606	0.051	-10.330	-29.851	-0.533	-1.636	0.001	-0.000	0.000	0.000
275.827	5	Q22	-15.3569	-0.244	1.860	-0.561	0.178	-10.696	-31.182	0.289	0.750	0.001	0.000	0.000	0.000
284.738	3			-5.244	3.448	-0.561	0.178	-8.116	-24.495	0.289	0.750	0.002	0.000	0.000	0.000
287.686	5	Q23	-23.5258	-7.931	4.619	-1.314	0.639	-5.945	-18.286	1.141	3.340	0.002	0.000	0.000	0.000
288.268	3			-8.695	4.991	-1.314	0.639	-5.281	-16.342	1.141	3.340	0.002	0.000	0.000	0.000
291.216	5	Q24	35.6874	-10.051	5.459	0.435	-0.336	-3.066	-10.096	0.427	1.081	0.002	-0.000	0.000	0.000
291.740	3			-9.823	5.283	0.435	-0.336	-2.842	-9.530	0.427	1.081	0.002	-0.000	0.000	0.000
292.740	4	B5	-0.7302	-9.388	4.947	0.435	-0.336	-2.415	-8.449	0.427	1.081	0.002	-0.000	-0.018	-0.036
299.187	3			-6.585	2.783	0.435	-0.336	0.340	-1.479	0.427	1.081	0.001	-0.000	-0.253	-0.036
307.213	3			-3.095	0.090	0.435	-0.336	3.770	7.198	0.427	1.081	-0.000	-0.000	-0.546	-0.036
310.161	5	Q25	-34.9404	-2.532	-0.963	-0.036	-0.409	3.996	8.344	-0.281	-0.337	-0.001	-0.000	-0.510	0.060
318.187	3			-2.824	-4.244	-0.036	-0.409	1.739	5.640	-0.281	-0.337	-0.004	-0.000	-0.029	0.060
319.187	4	B6	-1.2008	-2.860	-4.653	-0.036	-0.409	1.458	5.303	-0.281	-0.337	-0.004	-0.000	0.001	-0.000
320.187	3			-2.896	-5.062	-0.036	-0.409	1.177	4.966	-0.281	-0.337	-0.004	-0.000	0.000	-0.000
323.177	5	Q26	20.8870	-2.559	-5.452	0.256	0.155	0.480	4.700	-0.197	0.155	-0.004	0.000	0.000	-0.000
324.617	3			-2.191	-5.229	0.256	0.155	0.196	4.923	-0.197	0.155	-0.004	0.000	0.000	-0.000
327.607	5	Q27	-6.0930	-1.514	-5.000	0.200	0.000	-0.393	5.155	-0.194	-0.000	-0.004	0.000	-0.000	-0.000
329.047	3			-1.226	-5.000	0.200	0.000	-0.672	5.155	-0.194	-0.000	-0.004	0.000	-0.000	-0.000
335.047	3	RF2		-0.026	-5.000	0.200	0.000	-1.836	5.155	-0.194	-0.000	-0.004	0.000	-0.001	-0.000
336.579	3			0.280	-5.000	0.200	0.000	-2.133	5.155	-0.194	-0.000	-0.004	0.000	-0.001	-0.000
339.569	5	Q28	-41.7094	1.034	-6.640	0.330	-1.154	-2.024	3.631	0.263	-0.966	-0.005	-0.001	-0.001	0.000
341.009	3			1.510	-8.302	0.330	-1.154	-1.645	2.239	0.263	-0.966	-0.006	-0.001	-0.001	0.000
343.999	5	Q29	62.8536	1.695	-7.634	-0.216	1.565	-1.564	0.013	-0.205	-0.638	-0.005	0.001	-0.001	-0.000
345.439	3			1.383	-5.381	-0.216	1.565	-1.858	-0.906	-0.205	-0.638	-0.004	0.001	-0.001	-0.000
346.929	5	Q30	-25.8625	1.186	-3.500	-0.053	1.000	-1.977	-1.740	0.047	-0.464	-0.002	0.001	-0.001	0.000
349.929	3			1.027	-0.500	-0.053	1.000	-1.835	-3.133	0.047	-0.464	-0.000	0.001	-0.001	0.000
350.429	3	COLL		1.000	0.000	-0.053	1.000	-1.812	-3.365	0.047	-0.464	0.000	0.001	-0.001	0.000
350.929	3	COLL		0.973	0.500	-0.053	1.000	-1.788	-3.597	0.047	-0.464	0.001	0.001	-0.001	0.000
351.383	3			0.949	0.954	-0.053	1.000	-1.767	-3.807	0.047	-0.464	0.001	0.001	-0.001	0.000
351.783	3	TR6		0.928	1.354	-0.053	1.000	-1.748	-3.993	0.047	-0.464	0.001	0.001	-0.001	0.000

POSITION METERS	TYPE		STRENGTH T*M,T/M*M T/M**2*M	HORIZONTAL R11 MM/MM	R12 MM/MR	R21 MR/MM	R22 MR/MR	VERTICAL R33 MM/MM	R34 MM/MR	R43 MR/MM	R44 MR/MR	DISPERSION R16 MM/PC	R26 MR/PC	R36 MM/PC	R46 MR/PC
352.618	3			0.884	2.189	-0.053	1.000	-1.708	-4.381	0.047	-0.464	0.002	0.001	-0.001	0.000
354.618	4	B7	0.0000	0.778	4.189	-0.053	1.000	-1.614	-5.309	0.047	-0.464	0.003	0.001	-0.001	0.000
355.453	3			0.733	5.024	-0.053	1.000	-1.574	-5.696	0.047	-0.464	0.004	0.001	-0.001	0.000
355.853	3	TR7		0.712	5.424	-0.053	1.000	-1.555	-5.882	0.047	-0.464	0.004	0.001	-0.001	0.000
356.388	3			0.684	5.959	-0.053	1.000	-1.530	-6.130	0.047	-0.464	0.004	0.001	-0.001	0.000
359.378	5	Q31	61.6100	0.257	5.973	-0.210	-0.992	-2.125	-10.786	-0.476	-2.885	0.004	-0.001	-0.001	-0.000
360.818	3			-0.045	4.545	-0.210	-0.992	-2.810	-14.940	-0.476	-2.885	0.003	-0.001	-0.001	-0.000
363.766	5	Q32	-54.1184	-0.770	3.152	-0.314	-0.015	-2.986	-16.789	0.365	1.715	0.002	-0.000	-0.001	0.000
365.558	3			-1.332	3.125	-0.314	-0.015	-2.333	-13.717	0.365	1.715	0.002	-0.000	-0.001	0.000
368.506	5	Q33	3.3649	-2.216	3.004	-0.284	-0.067	-1.308	-8.962	0.334	1.525	0.002	-0.000	-0.000	0.000
369.946	3			-2.624	2.908	-0.284	-0.067	-0.827	-6.766	0.334	1.525	0.002	-0.000	-0.000	0.000
372.894	5	Q34	27.9124	-2.883	2.146	0.114	-0.432	0.051	-3.396	0.282	0.839	0.001	-0.000	-0.000	0.000
373.618	3			-2.800	1.834	0.114	-0.432	0.255	-2.788	0.282	0.839	0.001	-0.000	0.000	0.000
374.343	3			-2.718	1.521	0.114	-0.432	0.459	-2.180	0.282	0.839	0.001	-0.000	0.000	0.000
377.333	5	Q35	-8.8132	-2.550	0.302	-0.001	-0.392	1.254	0.417	0.244	0.879	-0.000	-0.000	0.000	0.000
378.689	3			-2.551	-0.229	-0.001	-0.392	1.584	1.609	0.244	0.879	-0.001	-0.000	0.001	0.000
381.678	5	Q36	35.3808	-1.907	-1.243	0.412	-0.256	2.816	4.918	0.616	1.431	-0.001	-0.000	0.001	0.000
383.118	3			-1.314	-1.612	0.412	-0.256	3.703	6.979	0.616	1.431	-0.001	-0.000	0.001	0.000
386.066	5	Q37	-59.3809	-0.534	-3.239	0.156	-0.927	3.762	7.774	-0.580	-0.932	-0.002	-0.001	0.001	-0.000
387.507	3			-0.309	-4.574	0.156	-0.927	2.927	6.432	-0.580	-0.932	-0.003	-0.001	0.001	-0.000
390.454	5	Q38	33.6388	0.187	-6.000	0.167	0.000	1.829	5.112	-0.196	-0.000	-0.004	0.000	0.001	-0.000
391.948	3			0.436	-6.000	0.167	0.000	1.537	5.112	-0.196	-0.000	-0.004	0.000	0.001	-0.000
392.348	3	TR8		0.503	-6.000	0.167	0.000	1.459	5.112	-0.196	-0.000	-0.004	0.000	0.001	-0.000
393.582	3			0.708	-6.000	0.167	0.000	1.217	5.112	-0.196	-0.000	-0.004	0.000	0.000	-0.000
394.582	3	TR9		0.875	-6.000	0.167	0.000	1.022	5.112	-0.196	-0.000	-0.004	0.000	0.000	-0.000
395.201	3			0.978	-6.000	0.167	0.000	0.901	5.112	-0.196	-0.000	-0.004	0.000	0.000	-0.000
397.467	3	XCED		1.356	-6.000	0.167	0.000	0.457	5.112	-0.196	-0.000	-0.004	0.000	0.000	-0.000
400.319	3	XCED		1.831	-6.000	0.167	0.000	-0.100	5.112	-0.196	-0.000	-0.004	0.000	0.000	-0.000
401.253	3			1.987	-6.000	0.167	0.000	-0.283	5.112	-0.196	-0.000	-0.004	0.000	-0.000	-0.000
401.253	3	XFS		1.987	-6.000	0.167	0.000	-0.283	5.112	-0.196	-0.000	-0.004	0.000	-0.000	-0.000
401.728	3			2.066	-6.000	0.167	0.000	-0.376	5.112	-0.196	-0.000	-0.004	0.000	-0.000	-0.000
402.528	5	Q39	-11.7752	2.249	-6.142	0.293	-0.356	-0.523	4.992	-0.169	-0.298	-0.004	-0.000	-0.000	-0.000
403.728	3			2.601	-6.569	0.293	-0.356	-0.725	4.634	-0.169	-0.298	-0.004	-0.000	-0.000	-0.000
404.528	5	Q40	11.7752	2.773	-6.697	0.134	0.036	-0.879	4.503	-0.216	-0.031	-0.004	0.000	-0.000	-0.000
405.023	3			2.839	-6.679	0.134	0.036	-0.986	4.488	-0.216	-0.031	-0.004	0.000	-0.000	-0.000
405.023	3	GTK1		2.839	-6.679	0.134	0.036	-0.986	4.488	-0.216	-0.031	-0.004	0.000	-0.000	-0.000
405.587	3			2.915	-6.659	0.134	0.036	-1.108	4.470	-0.216	-0.031	-0.004	0.000	-0.000	-0.000
408.087	4	B8	3.3356	3.251	-6.569	0.134	0.037	-1.648	4.393	-0.216	-0.031	-0.004	0.000	0.208	0.167
409.187	3			3.399	-6.529	0.134	0.037	-1.886	4.359	-0.216	-0.031	-0.004	0.000	0.391	0.167
411.687	4	B8	-3.3356	3.733	-6.435	0.134	0.037	-2.426	4.283	-0.216	-0.031	-0.004	0.000	0.599	-0.000
412.417	3			3.830	-6.408	0.134	0.037	-2.584	4.261	-0.216	-0.031	-0.004	0.000	0.599	-0.000
417.417	3	XCMV		4.499	-6.220	0.134	0.037	-3.664	4.107	-0.216	-0.031	-0.004	0.000	0.599	-0.000
417.907	3			4.564	-6.202	0.134	0.037	-3.770	4.092	-0.216	-0.031	-0.004	0.000	0.599	-0.000
417.907	3	GTK2		4.564	-6.202	0.134	0.037	-3.770	4.092	-0.216	-0.031	-0.004	0.000	0.599	-0.000
418.467	3			4.639	-6.181	0.134	0.037	-3.891	4.075	-0.216	-0.031	-0.004	0.000	0.599	-0.000
420.967	4	B9	-3.3356	4.973	-6.087	0.133	0.038	-4.431	3.998	-0.216	-0.031	-0.003	0.000	0.390	-0.167
422.067	3			5.120	-6.045	0.133	0.038	-4.669	3.964	-0.216	-0.031	-0.003	0.000	0.207	-0.167
424.567	4	B10	-3.3356	5.451	-5.948	0.133	0.039	-5.210	3.888	-0.216	-0.031	-0.003	0.000	-0.002	-0.000
425.678	3			5.598	-5.905	0.133	0.039	-5.450	3.853	-0.216	-0.031	-0.003	0.000	-0.002	-0.000
426.678	3	XCHV		5.731	-5.867	0.133	0.039	-5.666	3.823	-0.216	-0.031	-0.003	0.000	-0.002	-0.000
427.023	3			5.777	-5.853	0.133	0.039	-5.740	3.812	-0.216	-0.031	-0.003	0.000	-0.002	-0.000
427.423	4	TR11	-0.2402	5.830	-5.838	0.133	0.039	-5.827	3.800	-0.216	-0.031	-0.006	-0.012	-0.002	-0.000
427.823	3			5.883	-5.822	0.133	0.039	-5.913	3.788	-0.216	-0.031	-0.010	-0.012	-0.002	-0.000
427.823	3	GTK3		5.883	-5.822	0.133	0.039	-5.913	3.788	-0.216	-0.031	-0.010	-0.012	-0.002	-0.000
508.931	3			16.634	-2.675	0.133	0.039	-23.438	1.296	-0.216	-0.031	-0.979	-0.012	-0.008	-0.000
508.931	3	STR1		16.634	-2.675	0.133	0.039	-23.438	1.296	-0.216	-0.031	-0.979	-0.012	-0.008	-0.000
519.489	3			18.033	-2.265	0.133	0.039	-25.719	0.972	-0.216	-0.031	-1.106	-0.012	-0.008	-0.000
519.489	3	STR2		18.033	-2.265	0.133	0.039	-25.719	0.972	-0.216	-0.031	-1.106	-0.012	-0.008	-0.000
521.768	3			18.335	-2.177	0.133	0.039	-26.212	0.902	-0.216	-0.031	-1.133	-0.012	-0.009	-0.000
523.068	4	MNP	0.7205	18.507	-2.126	0.133	0.039	-26.493	0.862	-0.216	-0.031	-1.125	0.024	-0.009	-0.000
529.882	3			19.411	-1.862	0.133	0.039	-27.963	0.653	-0.216	-0.031	-0.961	0.024	-0.009	-0.000
529.882	3	STR3		19.411	-1.862	0.133	0.039	-27.963	0.653	-0.216	-0.031	-0.961	0.024	-0.009	-0.000
544.308	3			21.323	-1.302	0.133	0.039	-31.076	0.210	-0.216	-0.031	-0.614	0.024	-0.010	-0.000
544.308	3	STR4		21.323	-1.302	0.133	0.039	-31.076	0.210	-0.216	-0.031	-0.614	0.024	-0.010	-0.000
565.040	3			24.071	-0.497	0.133	0.039	-35.551	-0.427	-0.216	-0.031	-0.115	0.024	-0.012	-0.000
565.323	3	IRC		24.108	-0.486	0.133	0.039	-35.612	-0.436	-0.216	-0.031	-0.109	0.024	-0.012	-0.000
566.516	3			24.266	-0.440	0.133	0.039	-35.869	-0.473	-0.216	-0.031	-0.080	0.024	-0.012	-0.000
567.221	3	LKR		24.360	-0.413	0.133	0.039	-36.021	-0.494	-0.216	-0.031	-0.063	0.024	-0.012	-0.000
567.927	3	LKR		24.453	-0.385	0.133	0.039	-36.173	-0.516	-0.216	-0.031	-0.046	0.024	-0.012	-0.000
570.999	3			24.861	-0.266	0.133	0.039	-36.836	-0.610	-0.216	-0.031	0.028	0.024	-0.012	-0.000
570.999	3	XFB		24.861	-0.266	0.133	0.039	-36.836	-0.610	-0.216	-0.031	0.028	0.024	-0.012	-0.000
573.624	3			25.208	-0.164	0.133	0.039	-37.403	-0.691	-0.216	-0.031	0.091	0.024	-0.012	-0.000
575.624	4	B13	2.6418	25.471	-0.087	0.133	0.039	-37.836	-0.752	-0.213	-0.031	0.271	0.156	-0.012	-0.000
586.424	3			26.902	0.332	0.133	0.039	-40.131	-1.084	-0.213	-0.031	1.957	0.156	-0.013	-0.000
586.634	3	SAC		26.930	0.341	0.133	0.039	-40.175	-1.090	-0.213	-0.031	1.989	0.156	-0.013	-0.000
589.799	3			27.350	0.463	0.133	0.039	-40.848	-1.187	-0.213	-0.031	2.483	0.156	-0.013	-0.000
589.799	3	XWCM		27.350	0.463	0.133	0.039	-40.848	-1.187	-0.213	-0.031	2.483	0.156	-0.013	-0.000
590.424	3			27.433	0.488	0.133	0.039	-40.981	-1.206	-0.213	-0.031	2.581	0.156	-0.013	-0.000
593.224	3	DUMP		27.804	0.596	0.133	0.039	-41.576	-1.292	-0.213	-0.031	3.018	0.156	-0.014	-0.000
593.224	3			27.804	0.596	0.133	0.039	-41.576	-1.292	-0.213	-0.031	3.018	0.156	-0.014	-0.000

Transport from RF1 to RF2:

K12RFBEAM FOR NA62+ FR`om RF1 to RF2 TRANSPORT RUN15/12/20

POSITION METERS	TYPE		STRENGTH T*M,T/M*M T/M**2*M	HORIZONTAL R11 MM/MM	R12 MM/MR	R21 MR/MM	R22 MR/MR	VERTICAL R33 MM/MM	R34 MM/MR	R43 MR/MM	R44 MR/MR	DISPERSION R16 MM/PC	R26 MR/PC	R36 MM/PC	R46 MR/PC
0.000	3			1.000	0.000	0.000	1.000	1.000	0.000	0.000	1.000	0.000	0.000	0.000	0.000
3.000	3	RF1		1.000	3.000	0.000	1.000	1.000	3.000	0.000	1.000	0.000	0.000	0.000	0.000
5.000	3			1.000	5.000	0.000	1.000	1.000	5.000	0.000	1.000	0.000	0.000	0.000	0.000
7.000	5	Q9	18.7788	0.908	6.476	-0.091	0.453	1.095	7.540	0.097	1.579	0.000	0.000	0.000	0.000
16.000	3			0.089	10.553	-0.091	0.453	1.966	21.753	0.097	1.579	0.000	0.000	0.000	0.000
18.000	5	Q10	-21.5129	-0.089	12.647	-0.091	1.678	1.946	22.503	-0.117	-0.843	0.000	0.000	0.000	0.000
27.000	3			-0.908	27.750	-0.091	1.678	0.890	14.918	-0.117	-0.843	0.000	0.000	0.000	0.000
29.000	5	Q11	18.7788	-1.000	28.438	-0.000	-1.000	0.733	14.600	-0.042	0.521	0.000	0.000	0.000	0.000
45.280	3			-1.000	12.159	-0.000	-1.000	0.043	23.078	-0.042	0.521	0.000	0.000	0.000	0.000
47.280	5	Q12	-12.5930	-1.064	10.889	-0.064	-0.282	-0.043	22.661	-0.042	-0.934	0.000	0.000	0.000	0.000
63.703	3			-2.119	6.252	-0.064	-0.282	-0.739	7.330	-0.042	-0.934	0.000	0.000	0.000	0.000
65.703	5	Q13	10.8180	-2.131	5.362	0.052	-0.599	-0.865	5.828	-0.085	-0.581	0.000	0.000	0.000	0.000
82.126	3			-1.283	-4.477	0.052	-0.599	-2.266	-3.715	-0.085	-0.581	0.000	0.000	0.000	0.000
84.126	5	Q12	-12.5930	-1.259	-5.986	-0.027	-0.925	-2.292	-4.621	0.060	-0.316	0.000	0.000	0.000	0.000
100.549	3			-1.710	-21.175	-0.027	-0.925	-1.313	-9.812	0.060	-0.316	0.000	0.000	0.000	0.000
102.549	5	Q13	10.8180	-1.673	-21.858	0.065	0.249	-1.263	-10.990	-0.009	-0.873	0.000	0.000	0.000	0.000
118.972	3			-0.609	-17.773	0.065	0.249	-1.418	-25.331	-0.009	-0.873	0.000	0.000	0.000	0.000
120.972	5	Q14	-12.5930	-0.515	-18.395	0.030	-0.877	-1.348	-25.464	0.079	0.742	0.000	0.000	0.000	0.000
122.168	3			-0.480	-19.445	0.030	-0.877	-1.254	-24.577	0.079	0.742	0.000	0.000	0.000	0.000
123.168	4	B3	0.6574	-0.450	-20.322	0.030	-0.877	-1.175	-23.835	0.079	0.742	0.016	0.033	0.000	0.000
136.721	3			-0.046	-32.210	0.030	-0.877	-0.111	-13.781	0.079	0.742	0.462	0.033	0.000	0.000
139.669	5	Q15	35.7888	0.046	-26.451	0.030	4.611	0.111	-15.192	0.079	-1.741	0.434	-0.051	0.000	0.000
147.695	3			0.285	10.557	0.030	4.611	0.741	-29.162	0.079	-1.741	0.025	-0.051	0.000	0.000
148.695	4	B4	1.0207	0.315	15.167	0.030	4.611	0.820	-30.903	0.079	-1.741	-0.000	0.000	0.000	0.000
149.219	3			0.331	17.583	0.030	4.611	0.861	-31.815	0.079	-1.741	-0.000	0.000	0.000	0.000
152.167	5	Q16	-41.5851	0.534	38.272	0.115	10.134	0.819	-27.182	-0.105	4.722	-0.000	0.000	0.000	0.000
152.749	3			0.601	44.170	0.115	10.134	0.758	-24.434	-0.105	4.722	-0.000	0.000	0.000	0.000
155.697	5	Q17	32.1279	0.778	61.699	-0.000	1.285	0.608	-15.402	-0.000	1.645	0.000	0.000	0.000	0.000
164.608	3			0.778	73.151	-0.000	1.285	0.608	-0.744	-0.000	1.645	0.000	0.000	0.000	0.000
167.556	5	Q18	12.5069	0.708	70.189	-0.047	-3.264	0.665	4.186	0.039	1.751	0.001	0.000	0.000	0.000
176.468	3			0.287	41.104	-0.047	-3.264	1.014	19.789	0.039	1.751	0.001	0.000	0.000	0.000
179.416	5	Q19	-25.4771	0.195	38.827	-0.017	1.670	0.938	21.035	-0.089	-0.932	0.001	0.000	0.000	0.000
188.327	3			0.040	53.713	-0.017	1.670	0.144	12.730	-0.089	-0.932	0.002	0.000	0.000	0.000
191.275	5	Q20	10.1773	-0.012	54.539	-0.018	-1.117	-0.114	10.880	-0.088	-0.339	0.002	0.000	0.000	0.000
200.187	3			-0.174	44.586	-0.018	-1.117	-0.902	7.858	-0.088	-0.339	0.002	0.000	0.000	0.000
203.135	5	Q21	8.1070	-0.216	38.723	-0.010	-2.821	-1.222	7.313	-0.131	-0.035	0.002	-0.000	0.000	0.000
212.046	3			-0.306	13.583	-0.010	-2.821	-2.389	7.003	-0.131	-0.035	0.001	-0.000	0.000	0.000
214.994	5	Q22	-15.3569	-0.372	6.515	-0.036	-2.064	-2.495	6.127	0.060	-0.548	0.001	0.000	0.000	0.000
223.905	3			-0.690	-11.881	-0.036	-2.064	-1.960	1.241	0.060	-0.548	0.002	0.000	0.000	0.000
226.853	5	Q23	-23.5258	-0.924	-20.443	-0.128	-3.911	-1.463	-0.492	0.267	-0.594	0.002	0.000	0.000	0.000
227.435	3			-0.998	-22.719	-0.128	-3.911	-1.308	-0.838	0.267	-0.594	0.002	0.000	0.000	0.000
230.383	5	Q24	35.6874	-1.092	-27.550	0.067	0.778	-0.808	-2.975	0.086	-0.919	0.002	-0.000	0.000	0.000
230.907	3			-1.057	-27.143	0.067	0.778	-0.763	-3.456	0.086	-0.919	0.002	-0.000	0.000	0.000
231.907	4	B5	-0.7302	-0.989	-26.365	0.067	0.778	-0.676	-4.376	0.087	-0.919	0.002	-0.000	-0.018	-0.036
238.354	3			-0.557	-21.349	0.067	0.778	-0.118	-10.302	0.087	-0.919	0.001	-0.000	-0.253	-0.036
246.380	3			-0.018	-15.104	0.067	0.778	0.576	-17.680	0.087	-0.919	-0.000	-0.000	-0.546	-0.036
249.328	5	Q25	-34.9404	0.193	-16.665	0.082	-1.882	0.668	-15.806	-0.027	2.136	-0.001	-0.000	-0.510	0.060
257.354	3			0.849	-31.769	0.082	-1.882	0.451	1.337	-0.027	2.136	-0.004	-0.000	-0.029	0.060
258.354	4	B6	-1.2008	0.931	-33.651	0.082	-1.882	0.424	3.473	-0.027	2.136	-0.004	-0.000	0.001	-0.000
259.354	3			1.012	-35.533	0.082	-1.882	0.397	5.609	-0.027	2.136	-0.004	-0.000	0.000	-0.000
262.344	5	Q26	20.8870	1.090	-35.471	-0.031	1.923	0.376	13.231	0.012	3.094	-0.004	0.000	0.000	-0.000
263.784	3			1.046	-32.702	-0.031	1.923	0.394	17.686	0.012	3.094	-0.004	0.000	0.000	-0.000
266.774	5	Q27	-6.0930	1.000	-28.366	-0.000	1.000	0.413	25.999	-0.000	2.424	-0.004	0.000	-0.000	-0.000
268.214	3			1.000	-26.926	-0.000	1.000	0.413	29.490	-0.000	2.424	-0.004	0.000	-0.000	-0.000
274.214	3	RF2		1.000	-20.926	-0.000	1.000	0.413	44.034	-0.000	2.424	-0.004	0.000	-0.001	-0.000
275.746	3			1.000	-19.394	-0.000	1.000	0.413	47.748	-0.000	2.424	-0.004	0.000	-0.001	-0.000
278.736	5	Q28	-41.7094	1.328	-22.446	0.231	-3.147	0.291	40.146	-0.077	-7.242	-0.005	-0.001	-0.001	0.000
280.176	3			1.660	-26.977	0.231	-3.147	0.179	29.718	-0.077	-7.242	-0.006	-0.001	-0.001	0.000
283.166	5	Q29	62.8536	1.527	-23.276	-0.313	5.426	0.001	19.593	-0.051	-0.053	-0.005	0.001	-0.001	-0.000
284.606	3			1.076	-15.462	-0.313	5.426	-0.072	19.517	-0.051	-0.053	-0.004	0.001	-0.001	-0.000
286.096	5	Q30	-25.8625	0.700	-8.628	-0.200	3.894	-0.139	17.592	-0.037	-2.490	-0.002	0.001	-0.001	0.000
289.096	3			0.100	3.053	-0.200	3.894	-0.251	10.124	-0.037	-2.490	-0.000	0.001	-0.001	0.000
289.596	3	COLL		-0.000	5.000	-0.200	3.894	-0.269	8.879	-0.037	-2.490	0.000	0.001	-0.001	0.000
289.896	3	COLL		-0.060	6.168	-0.200	3.894	-0.280	8.132	-0.037	-2.490	0.000	0.001	-0.001	0.000

Beatch Listing:

K12RFBEAM - RF SEPARATED BEAM FOR NA62 V0.1

	X-COORDINATE	Y-COORDINATE	-COORDINATE	GISEMENT	HOR ANGLE	VERT ANGLE
INITIAL	768.31369	5099.39973	2445.49900	412.13068	1.380248	0.009165

I	ELEMENT		K	L	DEFL ANGLE	TILT	X	Y	Z	HOR ANGLE	VERT ANGLE	BEAM LENGTH
				M	RAD	DEG	M	M	M		RAD	M
1	T12	T12 (new T10)	20	0.000	0.000000	0.00	768.31369	5099.39973	2445.499	1.380248	0.009165	0.000
2			1	1.685			768.63281	5101.05416	2445.514	1.380248	0.009165	1.685
3		TCX	12	1.615	0.000000	0.00	768.93867	5102.63987	2445.529	1.380248	0.009165	3.300
4			1	0.450			769.02390	5103.08170	2445.533	1.380248	0.009165	3.750
5	QNR 101005	Q1	2	2.990			769.59017	5106.01746	2445.561	1.380248	0.009165	6.740
6			1	0.440			769.67351	5106.44948	2445.565	1.380248	0.009165	7.180
7	QNR 101009	Q2	2	2.990			770.23978	5109.38524	2445.592	1.380248	0.009165	10.170
8			1	0.655			770.36383	5110.02836	2445.598	1.380248	0.009165	10.825
9			1	0.555			770.46894	5110.57329	2445.603	1.380248	0.009165	11.380
10	QNR 101014	Q3	2	2.990			771.03522	5113.50905	2445.631	1.380248	0.009165	14.370
11			1	0.590			771.14695	5114.08835	2445.636	1.380248	0.009165	14.960
12			1	0.010			771.14885	5114.09816	2445.636	1.380248	0.009165	14.970
13	MTN 101018	B1	8	3.600	0.027008	0.01	771.78286	5117.64174	2445.669	1.407257	0.009155	18.570
14			1	3.030			772.27615	5120.63119	2445.697	1.407257	0.009155	21.600
15	DUMP101023	DUMP1	12	1.600	0.000000	0.00	772.53664	5122.20977	2445.712	1.407257	0.009155	23.200
16			1	0.010			772.53827	5122.21964	2445.712	1.407257	0.009155	23.210
17	DUMP101024	DUMP2	12	1.600	0.000000	0.00	772.79875	5123.79823	2445.726	1.407257	0.009155	24.810
18			1	0.380			772.86062	5124.17314	2445.730	1.407257	0.009155	25.190
19			1	0.300			772.90946	5124.46912	2445.733	1.407257	0.009155	25.490
20	MDXV101026	TRIM1	14	0.400	0.000000	0.00	772.97458	5124.86377	2445.736	1.407257	0.009155	25.890
21			1	0.300			773.02342	5125.15976	2445.739	1.407257	0.009155	26.190
22			1	0.200			773.05599	5125.35708	2445.741	1.407257	0.009155	26.390
23			1	0.040			773.06250	5125.39654	2445.741	1.407257	0.009155	26.430
24			1	0.000			773.06250	5125.39654	2445.741	1.407257	0.009155	26.430
25			1	0.291			773.10987	5125.68365	2445.744	1.407257	0.009155	26.721
26	QWL 101029	Q4	2	2.948			773.58982	5128.59219	2445.771	1.407257	0.009155	29.669
27			1	0.271			773.63394	5128.85956	2445.773	1.407257	0.009155	29.940
28	XCHV101030	C1,C2	12	1.000	0.000000	0.00	773.79675	5129.84618	2445.782	1.407257	0.009155	30.940
29			1	6.880			774.91684	5136.63410	2445.845	1.407257	0.009155	37.820
30	MTN 101040	B2	8	3.600	0.027008	0.01	775.45492	5140.19351	2445.878	1.434266	0.009144	41.420
31			1	0.633			775.54107	5140.82059	2445.884	1.434266	0.009144	42.053
32			1	0.000			775.54107	5140.82059	2445.884	1.434266	0.009144	42.053
33	QNL 101044	Q5	2	2.990			775.94801	5143.78264	2445.911	1.434266	0.009144	45.043
34			1	1.440			776.14399	5145.20918	2445.925	1.434266	0.009144	46.483
35	QNL 101048	Q6	2	2.990			776.55094	5148.17123	2445.952	1.434266	0.009144	49.473
36			1	1.440			776.74692	5149.59777	2445.965	1.434266	0.009144	50.913
37	QNL 101052	Q7	2	2.990			777.15386	5152.55983	2445.992	1.434266	0.009144	53.903
38			1	0.440			777.21375	5152.99571	2445.997	1.434266	0.009144	54.343
39	QTS 101055	Q8	2	1.490			777.41654	5154.47179	2446.010	1.434266	0.009144	55.833
40			1	0.500			777.48459	5154.96711	2446.015	1.434266	0.009144	56.333
41	XCHV101058	C3,C4	32	1.000	0.000000	0.00	777.62069	5155.95776	2446.024	1.434266	0.009144	57.333
42			1	0.500			777.68874	5156.45309	2446.028	1.434266	0.009144	57.833
43	RFCV101060	RF1	21	6.000	0.000000	0.00	778.50534	5162.39701	2446.083	1.434266	0.009144	63.833
44			1	2.000			778.77754	5164.37831	2446.102	1.434266	0.009144	65.833
45	QPL 101066	Q9	2	2.000			779.04974	5166.35962	2446.120	1.434266	0.009144	67.833
46			1	9.000			780.27465	5175.27549	2446.202	1.434266	0.009144	76.833
47	QPL 101077	Q10	2	2.000			780.54685	5177.25680	2446.220	1.434266	0.009144	78.833
48			1	9.000			781.77176	5186.17268	2446.303	1.434266	0.009144	87.833
49	QPL 101088	Q11	2	2.000			782.04396	5188.15398	2446.321	1.434266	0.009144	89.833
50			1	13.470			783.87723	5201.49807	2446.444	1.434266	0.009144	103.303
51	MDXV101101	TRIM 2	14	0.400	0.000000	0.00	783.93167	5201.89434	2446.448	1.434266	0.009144	103.703
52			1	0.410			783.98747	5202.30050	2446.452	1.434266	0.009144	104.113
53	XCSV101104	C5	11	1.000	0.000000	0.00	784.12357	5203.29116	2446.461	1.434266	0.009144	105.113
54			1	1.000			784.25967	5204.28181	2446.470	1.434266	0.009144	106.113
55	QPL 101107	Q12	2	2.000			784.53188	5206.26311	2446.488	1.434266	0.009144	108.113
56			1	16.423			786.76706	5222.53261	2446.638	1.434266	0.009144	124.536
57	QPL 101125	Q13	2	2.000			787.03926	5224.51391	2446.657	1.434266	0.009144	126.536
58			1	16.423			789.27444	5240.78340	2446.807	1.434266	0.009144	142.959
59	QPL 101144	Q12	1	2.000			789.54664	5242.76471	2446.825	1.434266	0.009144	144.959
60			1	16.423			791.78182	5259.03420	2446.975	1.434266	0.009144	161.382
61	QPL 101180	Q13	2	2.000			792.05402	5261.01551	2446.994	1.434266	0.009144	163.382
62			1	16.423			794.28920	5277.28500	2447.144	1.434266	0.009144	179.805
63	QPL 101180	Q14	2	2.000			794.56140	5279.26630	2447.162	1.434266	0.009144	181.805
64			1	1.196			794.72423	5280.45152	2447.173	1.434266	0.009144	183.001
65	MBPS101184	BEND3	8	1.000	0.003285	0.01	794.85871	5281.44239	2447.182	1.437551	0.009143	184.001
66			1	1.000			794.99155	5282.43349	2447.191	1.437551	0.009143	185.001
67			1	5.000			795.65578	5287.38896	2447.237	1.437551	0.009143	190.001
68			1	7.552			796.65903	5294.87371	2447.306	1.437551	0.009143	197.553
69	QWL 101200	Q15	2	2.948			797.05066	5297.79545	2447.333	1.437551	0.009143	200.501
70			1	8.027			798.11696	5305.75057	2447.406	1.437551	0.009143	208.528
71	MBPS101209	BEND4	8	1.000	0.005100	0.01	798.24728	5306.74200	2447.416	1.442651	0.009142	209.528
72			1	0.524			798.31424	5307.26169	2447.420	1.442651	0.009142	210.052
73	QWL 101212	Q16	2	2.948			798.69096	5310.18539	2447.447	1.442651	0.009142	213.000
74			1	0.582			798.76533	5310.76260	2447.453	1.442651	0.009142	213.582
75	QWL 101215	Q17	2	2.948			799.14206	5313.68630	2447.480	1.442651	0.009142	216.530
76			1	8.911			800.28084	5322.52427	2447.561	1.442651	0.009142	225.441
77	QWL 101227	Q18	2	2.948			800.65756	5325.44797	2447.588	1.442651	0.009142	228.389
78			1	8.911			801.79634	5334.28594	2447.669	1.442651	0.009142	237.301
79	QWL 101239	Q19	2	2.948			802.17306	5337.20964	2447.696	1.442651	0.009142	240.249
80			1	7.265			803.10150	5344.41517	2447.763	1.442651	0.009142	247.514
81	XCSV101247	C6	11	1.000	0.000000	0.00	803.22929	5345.40693	2447.772	1.442651	0.009142	248.514
82			1	0.646			803.31184	5346.04760	2447.778	1.442651	0.009142	249.160
83	QWL 101250	Q20	2	2.948			803.68856	5348.97131	2447.805	1.442651	0.009142	252.108
84			1	8.911			804.82734	5357.80927	2447.886	1.442651	0.009142	261.020
85	QWL 101263	Q21	2	2.948			805.20407	5360.73298	2447.913	1.442651	0.009142	263.968
86			1	8.911			806.34285	5369.57094	2447.995	1.442651	0.009142	272.879
87	QWL 101275	Q22	2	2.948			806.71957	5372.49465	2448.022	1.442651	0.009142	275.827
88			1	8.911			807.85835	5381.33261	2448.103	1.442651	0.009142	284.738
89	QWL 101285	Q23	2	2.948			808.23507	5384.25632	2448.130	1.442651	0.009142	287.686
90			1	0.582			808.30944	5384.83352	2448.135	1.442651	0.009142	288.268
91	QWL 101290	Q24	2	2.948			808.68617	5387.75723	2448.162	1.442651	0.009142	291.216
92			1	0.524			808.75313	5388.27691	2448.167	1.442651	0.009142	291.740
93	MBPS101291	BEND5	8	1.000	-0.003648	-89.98	808.88092	5389.26868	2448.174	1.442650	0.005494	292.740
94			1	4.473			809.45254	5393.70494	2448.199	1.442650	0.005494	297.213
95	XCMV101300	SCR1	11	5.000	0.000000	0.00	810.09151	5398.66387	2448.226	1.442650	0.005494	302.213

96			1	5.000			810.73048	5403.62280	2448.254	1.442650	0.005494	307.213
97	QWL 101309	Q25	2	2.948			811.10721	5406.54658	2448.270	1.442650	0.005494	310.161
98			1	1.800			811.33724	5408.33180	2448.280	1.442650	0.005494	311.961
99	MIB 101313	MIB1	23	3.200	0.000000	0.00	811.74618	5411.50551	2448.298	1.442650	0.005494	315.161
100			1	3.026			812.13288	5414.50665	2448.314	1.442650	0.005494	318.187
101	MBPS101319	BEND6	8	1.000	-0.006000	-89.98	812.26068	5415.49845	2448.317	1.442649	-0.000506	319.187
102			1	1.000			812.38847	5416.49025	2448.316	1.442649	-0.000506	320.187
103	QNL 101322	Q26	2	2.990			812.77059	5419.45573	2448.315	1.442649	-0.000506	323.177
104			1	1.440			812.95461	5420.88393	2448.314	1.442649	-0.000506	324.617
105	QNL 101336	Q27	2	2.990			813.33673	5423.84941	2448.312	1.442649	-0.000506	327.607
106			1	0.595			813.41277	5424.43953	2448.312	1.442649	-0.000506	328.202
107	XCHV101338	C7,C8	12	1.000	0.000000	0.00	813.54056	5425.43133	2448.312	1.442649	-0.000506	329.202
108			1	0.445			813.59743	5425.87268	2448.311	1.442649	-0.000506	329.647
109	RFCV101343	RF2	21	6.000	0.000000	0.00	814.36422	5431.82348	2448.308	1.442649	-0.000506	335.647
110			1	0.934			814.48358	5432.74982	2448.308	1.442649	-0.000506	336.581
111	QNL 101347	Q28	2	2.990			814.86569	5435.71531	2448.306	1.442649	-0.000506	339.571
112			1	1.440			815.04972	5437.14350	2448.306	1.442649	-0.000506	341.011
113	QNL 101351	Q29	2	2.990			815.43183	5440.10898	2448.304	1.442649	-0.000506	344.001
114			1	1.440			815.61586	5441.53717	2448.303	1.442649	-0.000506	345.441
115	QTS 101354	Q30	2	1.490			815.80628	5443.01496	2448.303	1.442649	-0.000506	346.931
116			1	3.000			816.18967	5445.99036	2448.301	1.442649	-0.000506	349.931
117	XCHV101358	C9,10	12	1.000	0.000000	0.00	816.31746	5446.98216	2448.301	1.442649	-0.000506	350.931
118			1	0.454			816.37548	5447.43243	2448.300	1.442649	-0.000506	351.385
119	MDXH101359	TRIM 3	13	0.400	0.000000	0.00	816.42660	5447.82915	2448.300	1.442649	-0.000506	351.785
120			1	0.835			816.53331	5448.65731	2448.300	1.442649	-0.000506	352.620
121	MBPL101362	BEND7 - IRON GAP	8	2.000	0.000000	0.00	816.78891	5450.64091	2448.299	1.442649	-0.000506	354.620
122			1	0.835			816.89562	5451.46906	2448.298	1.442649	-0.000506	355.455
123	MDXH101364	TRIM 4	13	0.400	0.000000	0.00	816.94674	5451.86578	2448.298	1.442649	-0.000506	355.855
124			1	0.535			817.01511	5452.39639	2448.298	1.442649	-0.000506	356.390
125	QNL 101367	Q31	2	2.990			817.39722	5455.36188	2448.296	1.442649	-0.000506	359.380
126			1	1.440			817.58125	5456.79007	2448.296	1.442649	-0.000506	360.820
127	QWL 101371	Q32	2	2.948			817.95799	5459.71390	2448.294	1.442649	-0.000506	363.768
128			1	1.792			818.18698	5461.49102	2448.293	1.442649	-0.000506	365.560
129	QWL 101375	Q33	2	2.948			818.56373	5464.41485	2448.292	1.442649	-0.000506	368.508
130			1	1.440			818.74776	5465.84304	2448.291	1.442649	-0.000506	369.948
131	QWL 101379	Q34	2	2.948			819.12450	5468.76687	2448.289	1.442649	-0.000506	372.896
132			1	1.448			819.30960	5470.20335	2448.289	1.442649	-0.000506	374.345
133	QNL 101384	Q35	2	2.990			819.69171	5473.16884	2448.287	1.442649	-0.000506	377.335
134			1	1.355			819.86488	5474.51273	2448.287	1.442649	-0.000506	378.690
135	QNL 101388	Q36	2	2.990			820.24699	5477.47821	2448.285	1.442649	-0.000506	381.680
136			1	1.440			820.43102	5478.90640	2448.284	1.442649	-0.000506	383.120
137	QWL 101392	Q37	2	2.948			820.80776	5481.83023	2448.283	1.442649	-0.000506	386.068
138			1	1.440			820.99179	5483.25842	2448.282	1.442649	-0.000506	387.508
139	QWL 101398	Q38	2	2.948			821.36854	5486.18225	2448.281	1.442649	-0.000506	390.456
140			1	0.446			821.42553	5486.62459	2448.280	1.442649	-0.000506	390.902
141	MDXH101400	TRIM8	13	0.400	0.000000	0.00	821.47665	5487.02131	2448.280	1.442649	-0.000506	391.302
142			1	0.500			821.54055	5487.51721	2448.280	1.442649	-0.000506	391.802
143	MDXH101400	TRIM9	14	0.400	0.000000	0.00	821.59167	5487.91393	2448.280	1.442649	-0.000506	392.202
144			1	1.210			821.74630	5489.11401	2448.279	1.442649	-0.000506	393.412
145	XCHV101401	C11,C12	12	1.000	0.000000	0.00	821.87410	5490.10581	2448.279	1.442649	-0.000506	394.412
146			1	0.791			821.97519	5490.89032	2448.278	1.442649	-0.000506	395.203
147	KTAG		1	0.425			822.02950	5491.31184	2448.278	1.442649	-0.000506	395.628
148		CEDAR Nose	1	0.348			822.07397	5491.65698	2448.278	1.442649	-0.000506	395.976
149	XCED101072		22	4.347	0.000000	0.00	822.62951	5495.96834	2448.276	1.442649	-0.000506	400.323
150			1	0.659			822.71373	5496.62194	2448.275	1.442649	-0.000506	400.982
151	XFFV101075	FISC 3	1	0.275			822.74887	5496.89468	2448.275	1.442649	-0.000506	401.257
152	XFFH101076	FISC 4	1	0.275			822.78401	5497.16743	2448.275	1.442649	-0.000506	401.532
153			1	0.200			822.80957	5497.36579	2448.275	1.442649	-0.000506	401.732
154	QFS 101077	Q39	3	0.800			822.91181	5498.15923	2448.274	1.442649	-0.000506	402.532
155			1	1.200			823.06517	5499.34939	2448.274	1.442649	-0.000506	403.732
156	QFS 101079	Q40	2	0.800			823.16741	5500.14283	2448.273	1.442649	-0.000506	404.532
157			1	0.470			823.22747	5500.60897	2448.273	1.442649	-0.000506	405.002
158	GTK 0		1	0.000			823.22747	5500.60897	2448.273	1.442649	-0.000506	405.002
159			1	0.050			823.23386	5500.65856	2448.273	1.442649	-0.000506	405.052
160	GTK 1		1	0.000			823.23386	5500.65856	2448.273	1.442649	-0.000506	405.052
161			1	0.135			823.25111	5500.79246	2448.273	1.442649	-0.000506	405.187
162	VAC.72x129		1	0.400			823.30223	5501.18918	2448.273	1.442649	-0.000506	405.587
163	MCBV101406	BEND8	8	2.500	0.000000	-89.98	823.62172	5503.66868	2448.272	1.442649	-0.000506	408.087
164			1	0.390			823.67156	5504.05548	2448.271	1.442649	-0.000506	408.477
165			1	0.038			823.67642	5504.09317	2448.271	1.442649	-0.000506	408.515
166	VXSV101083		1	0.058			823.68383	5504.15069	2448.271	1.442649	-0.000506	408.573
167			1	0.038			823.68869	5504.18838	2448.271	1.442649	-0.000506	408.611
168	VXRP		1	0.186			823.71246	5504.37285	2448.271	1.442649	-0.000506	408.797
169	VAC.72x129		1	0.390			823.76230	5504.75966	2448.271	1.442649	-0.000506	409.187
170	MCBV101412	BEND8	8	2.500	0.000000	-89.98	824.08179	5507.23916	2448.270	1.442649	-0.000506	411.687
171			1	0.400			824.13291	5507.63588	2448.270	1.442649	-0.000506	412.087
172			1	0.160			824.15336	5507.79457	2448.270	1.442649	-0.000506	412.247
173	GTK 2		1	0.000			824.15336	5507.79457	2448.270	1.442649	-0.000506	412.247
174			1	0.160			824.17381	5507.95325	2448.269	1.442649	-0.000506	412.407
175	VAC.152x55		1	0.330			824.21598	5508.28055	2448.269	1.442649	-0.000506	412.737
176	XCMV101416	SCR2	12	5.000	0.000000	0.00	824.85496	5513.23955	2448.267	1.442649	-0.000506	417.737
177			1	0.330			824.89714	5513.56684	2448.267	1.442649	-0.000506	418.067
178	VAC.72x129		1	0.400			824.94826	5513.96356	2448.266	1.442649	-0.000506	418.467
179	MCBV101419	BEND9	8	2.500	0.000000	-89.98	825.26775	5516.44306	2448.265	1.442649	-0.000506	420.967
180			1	0.390			825.31759	5516.82987	2448.265	1.442649	-0.000506	421.357
181	VAC. O=104		1	0.060			825.32526	5516.88937	2448.265	1.442649	-0.000506	421.417
182	VXSV101096		1	0.200			825.35082	5517.08773	2448.265	1.442649	-0.000506	421.617
183	VAC. O=104		1	0.060			825.35848	5517.14724	2448.265	1.442649	-0.000506	421.677
184	VAC.72x129		1	0.390			825.40833	5517.53404	2448.265	1.442649	-0.000506	422.067
185	MCBV101423	BEND10	8	2.500	0.000000	90.02	825.72782	5520.01354	2448.263	1.442649	-0.000506	424.567
186			1	0.400			825.77894	5520.41026	2448.263	1.442649	-0.000506	424.967
187	VXRP O=156		1	0.480			825.84028	5520.88633	2448.263	1.442649	-0.000506	425.447
188	Flange		1	0.010			825.84156	5520.89625	2448.263	1.442649	-0.000506	425.457
189	VAC(78x42)		1	0.120			825.85689	5521.01526	2448.263	1.442649	-0.000506	425.577
190	Flange		1	0.010			825.85817	5521.02518	2448.263	1.442649	-0.000506	425.587
191	TCX 101426		1	1.200			826.01153	5522.21534	2448.262	1.442649	-0.000506	426.787
192	Flange		1	0.010			826.01281	5522.22526	2448.262	1.442649	-0.000506	426.797
193	VAC(78x42)		1	0.030			826.01664	5522.25501	2448.262	1.442649	-0.000506	426.827
194	Flange		1	0.010			826.01792	5522.26493	2448.262	1.442649	-0.000506	426.837
195	VXBS		1	0.055			826.02495	5522.31948	2448.262	1.442649	-0.000506	426.892
196	VAC. O= 95		1	0.135			826.04220	5522.45337	2448.262	1.442649	-0.000506	427.027
197	MDXH101427	TRIM 11	13	0.400	0.000000	0.01	826.09332	5522.85009	2448.262	1.442649	-0.000506	427.427
198			1	0.235			826.12335	5523.08317	2448.262	1.442649	-0.000506	427.662
199	VAC. O=152		1	0.095			826.13549	5523.17739	2448.262	1.442649	-0.000506	427.757
200	VAC448x371		1	0.070			826.14444	5523.24681	2448.262	1.442649	-0.000506	427.827
201	GTK 3		1	0.000			826.14444	5523.24681	2448.262	1.442649	-0.000506	427.827
202			1	93.945			838.15032	5616.42148	2448.214	1.442649	-0.000506	521.772
203	MNP-33	B11,12 - MNP33	8	1.300	0.000000	0.01	838.31646	5617.71082	2448.213	1.442649	-0.000506	523.072
204			1	50.555			844.77724	5667.85128	2448.188	1.442649	-0.000506	573.627
205	MBPL101	BEND13 TAPERED	8	2.000	0.000000	0.01	845.03283	5669.83489	2448.187	1.442649	-0.000506	575.627
206			1	14.800			846.92423	5684.51353	2448.179	1.442649	-0.000506	590.427
207	BEAM DUMP	]	16	2.800	0.000000	0.00	847.28206	5687.29057	2448.178	1.442649	-0.000506	593.227

APPENDIX C: IMPACT OF BEAM MPMENTUM AND BEAM LENGTH on KAON DECAY RATE

For a given beam acceptance in angle and momentum, the kaon flux can be estimated from the 'Atherton formula' which parametrises the number N of K^+ produced at the target as

$$\frac{d^2N}{dp\,d\Omega} = A\left\{\frac{B}{p_o}e^{-Bp/p_o}\right\}\left\{\frac{Cp^2}{\pi}e^{-C(p\theta)^2}\right\}$$

per interacting proton per steradian and per GeV/c. For K^+, A = 0.16, B =8.5 and C = 3.0. More details are given e.g. in [5]. In our case the production angle θ = 0 and the primary proton momentum p_o is 400 GeV/c. Note that the beam optics defines a momentum acceptance in percent, which gives an extra factor proportional to the momentum p for increasing beam momentum. The fraction ε_T of incident protons that interacts in a 400 mm beryllium target (the target efficiency) is about 38%, Therefore formula for our case can be reduced to

$$\frac{d^2N}{dp\,d\Omega} = A\,\epsilon_T\left\{\frac{B}{p_o}e^{-Bp/p_o}\right\}\frac{Cp^2}{\pi}\,\frac{p}{100} = 1.23\;10^{-5}p^3e^{-p/47.05} \qquad \rightarrow 0.857\ (75\ GeV/c)\ or\ 0.742\ (60\ GeV/c)$$

where N is now the number of K^+ produced per incident proton, per steradian and per percent. However, once produced the kaons decay follow an exponential distribution with an average decay length of 7.52 m per GeV/c. Based on this formula, one can estimate the effect of a momentum change and of an increase of beam length.

In figure C.1 we show the fraction of K^+ at production within an angular acceptance of π μsterad and within a momentum spread of 1%. The maximum is at about 60 GeV/c.

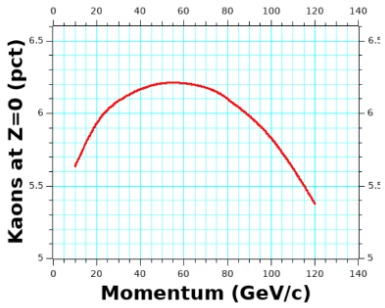

Figure C.1: *The faction of K^+ in the beam at production as a function of momentum*

However, due to decays, the K^+ rate is only relevant for a given start of the decay volume with respect to the production target. In NA62 the decay volume starts at≈ 105 m from the target. For that decay volume the kaon flux rises very rapidly with momentum. In fact, at very low momenta hardly any kaon survives until the start of the decay volume. See Figure C.2

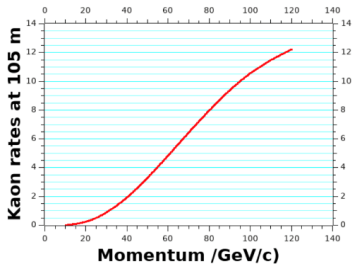

Figure C.2: *The kaon rate versus momentum at 105 m from the target within 1% and π μsterad acceptance*

More relevant for the experiment is the number of decays within a given decay volume, ≈ 60 m long for NA62. In Figure C.3 we show the number of decays between 105 and 165 metres as a function of momentum. Here we see an advantage for 75 GeV/c compared to 60 GeV/c by a factor of 1.39.

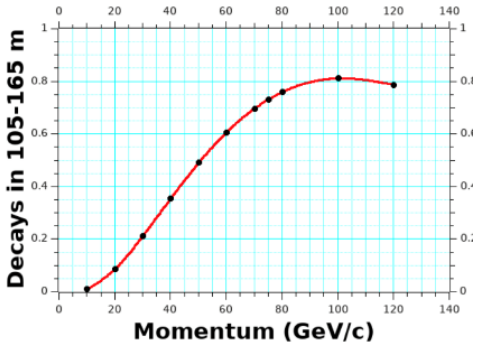

Figure C.3: *The number of K+ decays as a function of momentum for typical conditions*

If the beam (from target to start of fiducial volume) gets longer, the rate decreases, as well as the K^+ fraction, as K^+ decay much faster than π^+ (55 m/GeV/c) and protons are stable. In Figure C.4 we show the decrease of the K^+ fraction as a function of distance to the target for a beam momentum of 75 GeV/c.

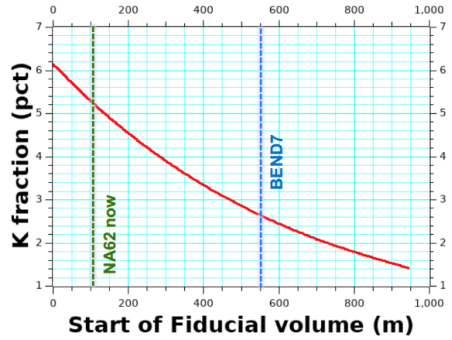

Figure C.4: *Fraction of K+ in the beam as a function of distance from the target (for 75 GeV/c)*

In Figure C.5 we show a comparison between the K^+ rate as a function of start of the fiducial volume for 60 and 75 GeV/c and in Figure C.6 the number of K^+ decays.

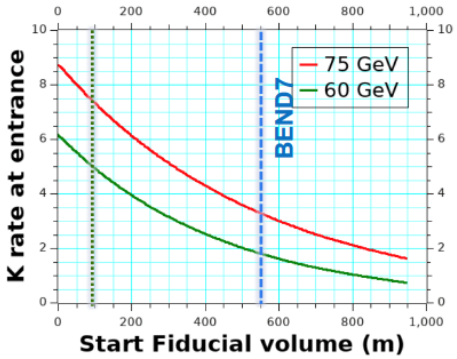

Figure C.5: *Comparison of the K^+ flux as a function of distance from the target to the start of the decay volume, for 60 and 75 GeV/c*

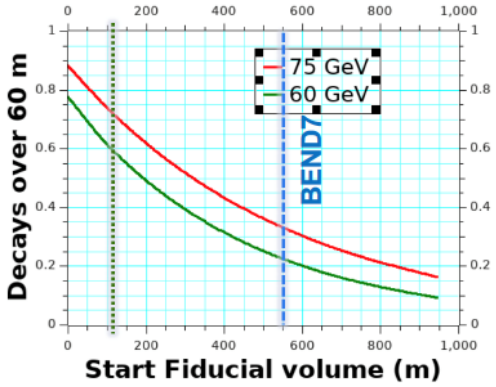

Figure C.6: *Comparison of the K^+ decay rate over 60 m as a function of distance from the target to the start of the decay volume, for 60 and 75 GeV/c*

The NA62 beam operates at 75 GeV/c and the fiducial volume starts at 105 m from the target. In the optics and layout described here the beam operates at 60 GeV/c and the decay volume starts at 428 m. For 75 GeV/c the loss due to distance would be about a factor 0.57 and for 60 GeV/c a factor 0.40. At 428 m the rate reduces to 72% by the decrease from 75 to 60 GeV/c. Overall the present layout would lose a factor of 2.4 for the same beam acceptance and the same incident proton flux. The consequence is that the acceptance of the new beam must be very close to that of the present beam and the RF losses must be much smaller than 50% if one wants to gain in K^+ flux. The natural K+ component (not counting e^+) decreases from 6.56% at 75 GeV/c at 135 m (centre of decay volume of NA62 now) to 3.35% for the long beam at 60 GeV/c. Therefore, a factor of 6 enrichment would bring the kaon fraction to 20%.